



This is a repository copy of *The importance of unsaturated hydraulic conductivity measurements for green roof detention modelling.*

White Rose Research Online URL for this paper:
<https://eprints.whiterose.ac.uk/163141/>

Version: Accepted Version

Article:

Peng, Z. orcid.org/0000-0003-3918-4479, Smith, C. and Stovin, V. (2020) The importance of unsaturated hydraulic conductivity measurements for green roof detention modelling. *Journal of Hydrology*. 125273. ISSN 0022-1694

<https://doi.org/10.1016/j.jhydrol.2020.125273>

Article available under the terms of the CC-BY-NC-ND licence
(<https://creativecommons.org/licenses/by-nc-nd/4.0/>).

Reuse

This article is distributed under the terms of the Creative Commons Attribution-NonCommercial-NoDerivs (CC BY-NC-ND) licence. This licence only allows you to download this work and share it with others as long as you credit the authors, but you can't change the article in any way or use it commercially. More information and the full terms of the licence here: <https://creativecommons.org/licenses/>

Takedown

If you consider content in White Rose Research Online to be in breach of UK law, please notify us by emailing eprints@whiterose.ac.uk including the URL of the record and the reason for the withdrawal request.



eprints@whiterose.ac.uk
<https://eprints.whiterose.ac.uk/>

1 **The importance of unsaturated hydraulic conductivity measurements for green roof**
2 **detention modelling**

3 Zhangjie Peng*, Colin Smith and Virginia Stovin

4 Department of Civil and Structural Engineering, The University of Sheffield, Mappin Street,
5 Sheffield S1 3JD, United Kingdom.

6 *Corresponding author

7 Email addresses: zpeng3@sheffield.ac.uk (Z. Peng), c.c.smith@sheffield.ac.uk (C. Smith),
8 v.stovin@sheffield.ac.uk (V. Stovin).

9 **Keywords:** Green roof substrate; Unsaturated hydraulic conductivity measurements;
10 Infiltration column; Detention modelling; Richards Equation.

11 **Abstract**

12 Characterising the unsaturated hydraulic conductivity of a green roof substrate is essential
13 for accurately modelling runoff detention in response to rainfall events. In this paper, the
14 unsaturated hydraulic conductivities for four representative green roof substrates were
15 determined in an infiltration column using steady state and transient techniques. The
16 conventional Durner-Mualem Hydraulic Conductivity Function (HCF) model, for which
17 parameters were calibrated based on the measured Soil Water Release Curve (SWRC) data,
18 was shown to provide a poor fit to the experimental data. A new three-segment HCF was,
19 therefore, proposed to fit measured unsaturated hydraulic conductivity data. Detention tests
20 were carried out on 100 mm and 200 mm deep substrates using four simulated storm events.

21 The runoff and moisture content data collected during the detention tests was used to
22 validate the HCFs using the Richards Equation. The new three-segment HCF resulted in
23 simulated runoff and moisture content profiles that closely matched the measured data (with
24 mean $R_t^2= 0.754$ for modelled runoff), in contrast to predictions made using the conventional
25 Durner-Mualem model (with mean $R_t^2=0.409$ for modelled runoff). It was also demonstrated
26 that further simplification of the HCF to a function defined by moisture content at just two
27 points – the saturated hydraulic conductivity and at an unsaturated hydraulic conductivity of
28 0.1 cm/min – provides a model that is fit-for-purpose for green roof runoff estimation (with
29 mean $R_t^2=0.629$ for modelled runoff).

30 1 Introduction

31 Green roofs provide stormwater management benefits through both retention and detention.
32 In this context, retention refers to rainfall that is held within the roof system and does not
33 leave the roof as runoff (i.e. initial losses). Retained rainfall may subsequently leave the roof
34 as evapotranspiration (Poë et al., 2015). Retention processes in green roofs are already well
35 understood from previous research (Fassman and Simcock, 2012; Liu and Fassman-Beck, 2016;
36 Poë et al., 2015; Stovin et al., 2013; Voyde et al., 2010).

37 Detention refers to the temporal delay that occurs between rainfall that is not retained hitting
38 the roof and emerging as runoff. Detention processes determine the timing and magnitude
39 of peak runoff to the downstream sewer network. Monitoring studies have demonstrated
40 that a green roof has the potential to delay the runoff peak and to reduce its magnitude
41 (Fassman-Beck et al., 2013; Stovin et al., 2012), which may help to mitigate the risk of localised
42 flooding and reduce the frequency of combined sewer overflows. Many previous studies on
43 detention focused on empirical analysis of monitored data, using different metrics to assess
44 the system's detention performance. However, these metrics do not directly lead to methods
45 that permit the modelling of green roof detention performance (Stovin et al., 2017).

46 Existing green roof detention modelling approaches include: empirical 'black-box' reservoir
47 routing models; a simplified physically-based model employed in the USEPA's Storm Water
48 Management Model (SWMM) (Rossman and Huber, 2016); and more sophisticated
49 unsaturated flow equations integrated into HYDRUS (Šimůnek et al., 2013). All these models
50 have shown acceptable levels of accuracy in modelling green roof detention (Bouzouidja et
51 al., 2018; Castiglia Feitosa and Wilkinson, 2016; Hilten et al., 2008; Kasmin et al., 2010; Liu
52 and Fassman-Beck, 2018; Palermo et al., 2019; Palla et al., 2009; Peng et al., 2019; Peng and

53 Stovin, 2017; Soulis et al., 2017). The parameters in empirical models have no direct link to
54 green roof components (Stovin et al., 2015); they have to be calibrated for different
55 configurations. On the other hand, the parameters required to run a physically-based (i.e.
56 Richards Equation) model are linked to the system's physical properties and such models are
57 therefore potentially more generic in their application (Peng et al., 2019). However, the
58 Richards Equation depends upon models and assumptions derived from natural soils that may
59 not be fully applicable within green roof substrates, which are typically heterogeneous,
60 coarse-grained, engineered media.

61 The two essential properties that need to be characterised to utilise Richards Equation based
62 models are the Soil Water Release Curve (SWRC) and a Hydraulic Conductivity Function (HCF)
63 (Richards, 1931). The SWRC describes the substrate's ability to hold water as a function of the
64 suction head. The method of determining SWRC is straightforward: water is extracted from
65 the substrate by applying increasing pressure. Many studies have determined and reported
66 SWRC for green roof substrates (Berretta et al., 2014; Liu and Fassman-Beck, 2018, 2017; Peng
67 et al., 2019; Sims et al., 2019). Two SWRC models that were originally derived for natural soils
68 – the van Genuchten (van Genuchten, 1980) and Durner (Durner, 1994) models – have been
69 shown to fit the measured SWRC data for green roof substrates, with some evidence that the
70 Durner model represents the SWRC of green roof substrates more accurately (Brunetti et al.,
71 2016; Liu and Fassman-Beck, 2018, 2017; Peng et al., 2019). Note that the models referred
72 to here are presented in full later in the paper.

73 The HCF is a function that describes the variation of hydraulic conductivity with soil moisture
74 content in variably saturated substrates. Unsaturated hydraulic conductivity determines the
75 speed of the water flowing through the substrate; it influences the time the runoff starts, the

76 peak runoff rate and the duration of the runoff. Through a series of sensitivity analyses, Peng
77 et al. (2019) demonstrated that the HCF has a considerable influence on model results (e.g. a
78 50% reduction in peak runoff was witnessed when a different HCF was used). However, few
79 studies have attempted to measure this property for green roof substrates directly. Brunetti
80 et al. (2016) determined the HCF for a green roof substrate using a Hyprop (a device for SWRC
81 and HCF determinations). As the water flow in the substrate is driven by evaporation during
82 the Hyprop test, the unsaturated hydraulic conductivity was only determined at low moisture
83 contents. However, when detention occurs in a green roof during storm events, the moisture
84 content within the substrate is typically between field capacity and saturation (Fassman and
85 Simcock, 2012; Liu and Fassman-Beck, 2018; Peng et al., 2019); therefore the hydraulic
86 conductivity in this range is more relevant for detention performance (Peng et al., 2019). Liu
87 and Fassman-Beck (2018) determined the unsaturated hydraulic conductivity for seven green
88 roof substrates consisting of pumice, zeolite and sand, using a small diameter infiltration
89 column. Data points on the HCF near field capacity were obtained under steady-state and
90 transient conditions. However, tensiometers were not included in the experiment, so the
91 suction head, which is needed for hydraulic conductivity calculations under transient
92 conditions, was not directly measured. Instead, it was estimated from the substrate's SWRC.
93 There is, therefore, a clear need for improved HCF data for green roof substrates, particularly
94 in the range of moisture content between field capacity and saturation.

95 For natural soils, SWRC models are typically combined with the Mualem equation (Mualem,
96 1976) to estimate the HCF. However, this approach has met with varying levels of success
97 when compared to measured HCF data points for green roof substrates. Whilst Brunetti et al.
98 (2016) concluded that the Durner-Mualem approach accurately represented the HCF for a
99 green roof substrate comprising 74% gravel, 22% sand, and 4% silt and clay, Liu and Fassman-

100 Beck (2018) reached the opposite conclusion with the substrates they studied. Peng et al.
101 (2019) also highlighted the poor fit of a Durner-Mualem model to preliminary laboratory HCF
102 measurements for a crushed brick-based green roof substrate. Other HCF models (e.g.
103 Campbell, 1974) are available for unsaturated hydraulic conductivity estimations. However,
104 these models have not been validated or applied to green roof substrate detention modelling
105 in any previous work.

106 Given the limited availability of measured HCF data, most Richards equation-based studies to
107 date have applied the Durner-Mualem or van Genuchten-Mualem models to represent the
108 HCF for green roof substrates (Brunetti et al., 2016; Castiglia Feitosa and Wilkinson, 2016; Liu
109 and Fassman-Beck, 2017; Palla et al., 2012, 2009; Peng et al., 2019; Sims et al., 2019; Soulis et
110 al., 2017). Brunetti et al. (2016) compared the model results of van Genuchten-Mualem and
111 Durner-Mualem based on more than a month of green roof rainfall-runoff data and concluded
112 that both models provided reasonable predictions of the runoff profiles. Further investigation
113 of the Durner-Mualem model was conducted with a single rainfall event, and the model was
114 shown to regenerate the runoff profile accurately. Peng et al. (2019) used the Durner-Mualem
115 model within the Richards Equation to generate runoff profiles from a green roof test bed
116 consisting of 80 mm (thickness) substrate overlying a 25 mm (thickness) drainage layer in
117 response to five real rainfall events. The model showed a reasonable prediction of runoff.
118 Whilst these cases appear to validate the applicability of the Durner-Mualem model; they are
119 based on runoff data from full green roof systems typically comprising vegetation and
120 drainage layers in addition to the substrate layer. Such data does not therefore provide a
121 direct validation for the correct representation of the substrate layer.

122 Liu and Fassman-Beck (2017) validated the Durner-Mualem model for green roof substrates
123 alone. They used the Durner-Mualem approach to model the runoff from five 100 mm green
124 roof substrates. The model was capable of predicting the peak runoff; however, the rising and
125 falling limbs of the runoff profiles were poorly modelled, indicating a poor representation of
126 detention processes. The model's poor performance was attributed to preferential flow.
127 However, given that the authors noted that the Durner-Mualem HCF used in the model did
128 not accurately represent the HCF for green roof substrates, this may also have contributed to
129 the observed discrepancies.

130 Green roof detention models have typically been validated based on runoff data from either
131 the substrate or the whole system (Kasmin et al., 2010; Liu and Fassman-Beck, 2017; Palla et
132 al., 2009, 2012; Vesuviano et al., 2014; Yio et al., 2013). However, the vertical moisture
133 content profiles, which reflect the volume of water temporarily stored in the substrate,
134 provide valuable insights into the performance of an unsaturated flow model (Peng et al.,
135 2019). Palla et al. (2009) validated the Richards Equation from the perspective of vertical
136 moisture content profile. However, only a few points in time were compared with measured
137 data. Peng et al. (2019) utilised continuous time-series moisture content data measured at
138 three different depths within a substrate to validate the Richards Equation; it was found that
139 the Richards Equation tended to slightly overestimate the vertical moisture content gradient.

140 The aim of this study is to understand the variations of hydraulic conductivity within green
141 roof substrates during storm events and to facilitate improved modelling of the detention
142 effects within the substrate using the Richards Equation. The aim is achieved via the following
143 objectives:

- 144 • Experimentally characterise the basic physical properties and Soil Water Release
145 Curve (SWRC) of four representative green roof substrates;
- 146 • Evaluate the applicability of existing SWRC models for green roof substrates;
- 147 • Experimentally measure unsaturated hydraulic conductivities for the representative
148 green roof substrates;
- 149 • Assess the capability of existing Hydraulic Conductivity Function models to represent
150 the hydraulic conductivity characteristics of green roof substrates;
- 151 • Characterise the green roof substrates' runoff and moisture content profiles in
152 response to various design storms;
- 153 • Compare the abilities of alternative Hydraulic Conductivity Functions to reproduce
154 observed runoff and vertical moisture content profiles;
- 155 • Propose a simplified approach for measuring and deriving Hydraulic Conductivity
156 Functions for green roof substrates.

157 **2 Methods**

158 **2.1 Trial substrates**

159 Three representative green roof substrates from an external supplier and a homemade green
160 roof substrate mixture were used in this study. Heather with Lavender Substrate (HLS) and
161 Sedum Carpet Substrate (SCS) are manufactured by ZinCo, whereas the Marie Curie Substrate
162 (MCS) was a comparable substrate developed between the University of Sheffield and ZinCo
163 as part of a collaborative research project. These three substrates have been used in previous
164 experimental and field studies, and they have shown the potential to provide hydrological
165 benefits (Berretta et al., 2014; De-Ville et al., 2017; Stovin et al., 2015; Yio et al., 2013). The
166 New Substrate Mix (NSM) is a homemade substrate that was designed to contain a higher

167 percentage of fines. This was done with the intention of developing a substrate that would
168 have contrasting SWRC and HCF characteristics compared to the other materials. The
169 components of NSM were separated out from HLS by sieving. As the organic matter was lost
170 during the preparation processes, 5% (v/v) of John Innes No.1 compost was added to the
171 mixture. Fig. 1 shows photographs of the four green roof substrates. MCS shows the highest
172 proportion of large particles. There is no significant difference between HLS and SCS, but as
173 HLS contains perlite, it looks whiter than SCS; NSM contains more fines.

174 **Fig. 1.**

175 **2.2 Experimental set up**

176 **2.2.1 Substrate basic characteristics**

177 The Forschungsgesellschaft Landschaftsentwicklung Landschaftsbau (FLL) (FLL, 2008) is a
178 standard guidance for determining selected green roof substrate physical properties. The FLL
179 outlines laboratory test methods, apparatus, and standard target values for substrates to
180 achieve their design functions. In this study, properties determined for the substrates using
181 the FLL methods included particle size distribution (PSD), d_{50} , bulk density, porosity, maximum
182 water holding capacity (MWHC) and water permeability (saturated hydraulic conductivity).

183 **2.2.2 Soil Water Release Curve (SWRC)**

184 The Soil Water Release Curve (SWRC) is determined by measuring paired values of suction
185 head and moisture content. In this study, similar to the methods adopted in Liu and Fassman-
186 Beck (2018), the hanging column (Carter and Gregorich, 2007) method was used to
187 characterise the SWRC at low suction heads, and the pressure extractor (Carter and Gregorich,
188 2007) method was used to determine the curve at high suction heads. For the hanging column,

189 a 100 mm (diameter) × 100 mm (height) plastic ring was used to hold the substrate.
190 Considering the specific characteristics of green roof substrates, a wet strengthened filter
191 sheet was attached to the base of the ring to avoid sample residues on the ceramic plate at
192 the end of the test (Fig. C.1, Supplementary Material C). The characterisations started with
193 saturated samples and 11 successive suction heads (6 cm to 100 cm) were applied to the
194 substrate samples to construct the SWRC. An equilibrium state was judged to have been
195 attained when water stopped leaving the substrate for four hours and the water in the
196 reservoir started to move backwards to the substrate samples. The samples were weighed
197 after they reached equilibrium state and then the suction head was increased. When samples
198 reached equilibrium at the final suction head, they were transferred to steel trays and dried
199 in the oven at 105°C for 24 hours to determine the sample dry weights and to calculate
200 moisture content at each suction head. Three replications were conducted for each substrate
201 to minimise the uncertainties associated with subsampling. The data points measured by the
202 pressure extractor method were adopted from previous studies (Berretta et al., 2014). As
203 pressure extractor data for the NSM was unavailable, all the SWRC data for this substrate was
204 determined by the hanging column method, with two additional suction heads at 200 cm and
205 300 cm.

206 **2.2.3 Hydraulic Conductivity Function (HCF)**

207 The infiltration column, drainage column and evaporation column methods (ASTM, 2010),
208 were modified to measure the HCF for green roof substrates. Each method applies to a
209 specific range of moisture contents; in combination, they permit the full HCF curve to be
210 characterised.

211 The infiltration method is particularly suitable for characterisation at high moisture contents.
212 Water infiltrates from the surface of the substrate, wetting the initially air dried substrate and
213 subsequently generating outflow from the bottom. The drainage column and evaporation
214 column methods were adopted specifically for the measurements of HCF at low moisture
215 contents. Without any inflow imposed to the substrate, water is lost from the substrate
216 through drainage and/or evaporation. These methods involve continuous measurements of
217 a vertical profile of moisture content and suction head.

218 Fig. 2 illustrates the apparatus used for HCF determinations. The apparatus comprises an
219 infiltration flow control system, sample column, moisture content measurement devices,
220 suction head measurement devices and an outflow measurement system. Inspired by the
221 experimental set up of Yio et al. (2013), the infiltration rate was controlled by a peristaltic
222 pump. In this study, 11 steady infiltration rates, ranging from 0.014 cm/min to 1.41 cm/min,
223 were applied to the substrates. Hypodermic needles (BD, Microlance 3 26G and 21G) were
224 used to distribute the water evenly to the substrate surface. The small needles (26G) are
225 capable of distributing a low flow rate (≤ 0.14 cm/min), and the large needles (21G) are
226 suitable for high flowrates (> 0.14 cm/min). The sample column is 540 mm high and has a
227 diameter of 300 mm. The height was chosen to ensure that there is a volume of substrate
228 that is not influenced by the boundary conditions and the diameter was chosen to minimise
229 wall effects (preferential flow). A perforated base covered by a layer of mesh and filter sheet
230 (Zinco, Systemfilter SF) was placed above a funnel. A runoff collecting barrel with a pressure
231 transducer (Druck Inc. PDCR 1830) was used to measure water depth in a straight-sided
232 collection barrel, which was subsequently used to determine the outflow from the substrate.
233 Five moisture probes (P1 to P5, Meter, 5TM, with an accuracy of ± 0.03 v/v) and three
234 tensiometers (T1 to T3, Meter, T5x, with an accuracy of ± 5 cm) were placed at different depths

235 to measure the change in moisture content and suction head respectively. The moisture
236 probes were put into place while the column was being filled with substrates, and the
237 substrate around the probes was gently pressed in place to obtain a good hydraulic
238 connection. Considering the strength of the apparatus, no compaction was applied to the
239 substrate. To avoid water losses from the tensiometer reservoir in the dry substrate, the
240 tensiometers were inserted into the substrate once the substrate had reached steady state
241 under the lowest flowrate. The moisture probes were connected to a Meter Em50 data
242 logger, whilst the tensiometers and pressure transducers were connected to a Campbell
243 Scientific CR1000 data logger. Continuous readings from the sensors were recorded at 1-
244 minute time intervals. Before tests, the moisture probes were calibrated for each substrate,
245 and the depth versus pressure relationship was calibrated for the collection barrel.

246 **Fig. 2.**

247 Two samples of each substrate were used to characterise each of the four green roof
248 substrates and it took approximately five weeks of measurements to complete each HCF. Two
249 techniques, steady state and transient, were adopted to determine the unsaturated hydraulic
250 conductivities.

251 The steady state condition applies when moisture content does not change with time or with
252 depth, and water flow is driven only by gravity. In this state, as no gradient is present with
253 depth, the hydraulic conductivity is equal to the imposed infiltration rate or the outflow rate
254 (ASTM, 2010; Liu and Fassman-Beck, 2018). However, due to the heterogeneous nature of
255 green roof substrates, variations between probe readings at specific positions in the substrate
256 are always present; in this study steady state was judged to be attained when the change in
257 moisture content over an hour at all five depths was less than 0.0008 v/v. 0.0008 v/v is the

258 resolution of the moisture probes. Outflow measurements were conducted once a steady
259 state had been attained. Limited by the capacity of the collecting barrel, the duration for the
260 outflow measurement was between 5 minutes and 1 hour, depending on the infiltration rate
261 imposed on the substrate. To exclude the influence of boundary conditions, the moisture
262 contents measured by the topmost and bottommost probes were excluded from the analysis.
263 The measured moisture contents from the remaining three probes at steady state were
264 averaged to provide the mean moisture content corresponding to each outflow rate. The
265 infiltration rate was then increased and the process repeated until the final measurement at
266 1.41 cm/min had been taken.

267 In the transient (or instantaneous profile) method, the unsaturated hydraulic conductivity is
268 calculated using the transient measurements of moisture content and suction head. This
269 method applies to the drainage and evaporation column methods. The transient
270 measurements were conducted under conditions of no inflow, after all the steady state
271 measurements were finished. The column used to hold substrate has a perforated base, so
272 when inflow stops, drainage occurs initially, followed by evaporation later on. The total head
273 at two adjacent vertical points (the two points where the tensiometers and moisture probes
274 are) was calculated from measured suction heads to determine the direction of flow, and then
275 the measured data was used to calculate the hydraulic conductivity based on Darcy's Law
276 (ASTM, 2010). The calculated hydraulic conductivity was then correlated with the mean
277 moisture content averaged over the two adjacent points.

278 Detailed descriptions of the steady-state and transient techniques can be found in
279 Supplementary Material A.

280 **2.2.4 Detention tests**

281 The apparatus used for HCF characterisations (Fig. 2) was also used for the detention tests.
282 To represent typical green roof system build-ups, detention tests were conducted on 100 mm
283 and 200 mm deep substrates. To evaluate substrate detention performance in response to
284 various rainfall intensities and rainfall profiles, four design storms were applied to the
285 substrates. In Design Storms 1, 2 & 3 respectively, 0.1, 0.37 and 0.51 mm/min constant rainfall
286 was applied to the substrates for 30 minutes. These intensities are equivalent to the
287 intensities associated with one-hour 1 in 1, 10 and 30 years Sheffield (UK) rainfall (NERC, 1999).
288 As the response at the start and the end of the event is of interest, the design storms were
289 applied for a reduced duration of 30 minutes. Design storm 4 is a storm profile with 9.2 mm
290 of total rainfall distributed over five 6-minute time-steps according to the UK 75% summer
291 profile (NERC, 1975). Before each test, the substrate was placed in the column and levelled
292 off without compaction. The substrate was initially wetted with 1.2 mm/min of rainfall for 2
293 hours, and it was then left to drain for 2 hours to ensure that it was at field capacity (FLL, 2008;
294 Yio et al., 2013). The moisture content measured by the lowest moisture probe at field
295 capacity was recorded, then a design storm was applied to the substrate for 30 minutes. Three
296 replications were conducted. As high levels of consistency were observed (the mean Standard
297 Deviation of each test for the three replications can be found in Table C.2, Supplementary
298 Material C), the results presented are the mean results. Without changing the layout of the
299 column, the lowest moisture probe was used to record the moisture change in the 100 mm
300 substrates during the detention tests. The moisture content measurements recorded by the
301 two lowest moisture probes in the 200 mm substrates make it possible to investigate the
302 vertical moisture content gradients within the substrates during the storms. Runoff from the

303 bottom of the substrate was recorded by the pressure transducer in the collecting barrel.
 304 Control tests were conducted without a substrate component; the runoff collected from the
 305 control tests was used as rainfall input to the model described in Section 2.4. The data
 306 collected during the detention tests was used to evaluate the detention performance of the
 307 substrates and to validate the model.

308 **2.3 Detention modelling**

309 The 1-D vertical Richards Equation (Eq. 1) (Richards, 1931) was used to model the runoff and
 310 the vertical moisture content profiles for the substrates in response to the design storms.

$$311 \quad \frac{\partial \theta}{\partial t} = \frac{\partial}{\partial Z} [K(h) \left(\frac{\partial h}{\partial Z} - 1 \right)] \quad (1)$$

312 where θ (v/v) is moisture content, $K(h)$ is hydraulic conductivity (cm/min) at suction head h
 313 (cm) and Z (cm) is the elevation of the point relative to the reference level. To solve the
 314 Richards Equation, SWRC and HCF are needed. The van Genuchten model (van Genuchten,
 315 1980) for SWRC is presented in Eq. 2 and the van Genuchten-Mualem model is shown in Eq.
 316 3 (Mualem, 1976). The Durner equation has been shown to provide good representation of
 317 the SWRC for green roof substrates (Liu and Fassman-Beck, 2017; Peng et al., 2019). Therefore,
 318 to validate the conventional approach to using the Richards Equation, the Durner equation
 319 (Durner, 1994) (Eq. 4) was used to represent the SWRC, and the Durner-Mualem equation
 320 (Mualem, 1976) (Eqs. 5-7) was used to estimate unsaturated hydraulic conductivity as a
 321 function of the suction head.

$$322 \quad S_e = \frac{\theta - \theta_r}{\theta_s - \theta_r} = [1 + (\alpha h)^n]^{-m} \quad (2)$$

$$323 \quad K(S_e) = K_s S_e^{0.5} [1 - (1 - S_e^{1/m})^m]^2 \quad (3)$$

324
$$S_e = \frac{\theta - \theta_r}{\theta_s - \theta_r} = w[1 + (\alpha_1 h)^{n_1}]^{-m_1} + (1 - w)[1 + (\alpha_2 h)^{n_2}]^{-m_2} \quad (4)$$

325
$$S_{e_1} = [1 + (\alpha_1 h)^{n_1}]^{-m_1} \quad (5)$$

326
$$S_{e_2} = [1 + (\alpha_2 h)^{n_2}]^{-m_2} \quad (6)$$

327
$$K(S_e) = K_s(wS_{e_1} + (1 - w)S_{e_2})^\tau \times \frac{\left\{ w\alpha_1 \left[1 - \left(1 - S_{e_1}^{1/m_1} \right)^{m_1} \right] + (1 - w)\alpha_2 \left[1 - \left(1 - S_{e_2}^{1/m_2} \right)^{m_2} \right] \right\}^2}{(w\alpha_1 + (1 - w)\alpha_2)^2} \quad (7)$$

328 where S_e , S_{e_1} or S_{e_2} is the relative saturation (-), θ is moisture content (v/v), θ_r is residual
 329 moisture content (v/v), θ_s is saturated moisture content (v/v), h is suction head (cm), α , n , m ,
 330 w , α_1 , n_1 , m_1 , α_2 , n_2 , m_2 are empirical parameters, α is the inverse of air-entry value (m^{-1}), n
 331 is a pore size distribution index (-) and $m = 1 - \frac{1}{n}$, K_s is saturated hydraulic conductivity
 332 (cm/min), $K(S_e)$ is the unsaturated hydraulic conductivity (cm/min) at S_e , $K(\theta)$ is the
 333 unsaturated hydraulic conductivity (cm/min) at θ , τ is the tortuosity parameter and is
 334 assumed to be 0.5.

335 The functions described above provide estimates of the HCF for situations in which directly
 336 measured unsaturated hydraulic conductivities are not available. New continuous functions
 337 were required to enable the directly measured data to be input into the detention model.
 338 When the measured unsaturated hydraulic conductivity data was plotted on a logarithmic
 339 axis, it was observed that a linear relationship with moisture content was evident. Up to two
 340 discontinuities in this linear relationship were noted, leading to the proposal to fit a three-
 341 segment exponential function to the measured data (Eqs. 8-10):

342
$$\text{if } \theta_1 < \theta \leq \theta_s; \quad K(\theta) = 10^{\beta_1 \cdot \theta + \gamma_1} \quad (8)$$

343
$$\text{if } \theta_2 < \theta \leq \theta_1; \quad K(\theta) = 10^{\beta_2 \cdot \theta + \gamma_2} \quad (9)$$

344 if $\theta < \theta_2$; $K(\theta) = 10^{\beta_3 \cdot \theta + \gamma_3}$ (10)

345 where θ_1, θ_2 are the two intercepts (v/v) on the HCF, $\beta_1, \gamma_1, \beta_2, \gamma_2, \beta_3$ and γ_3 are empirical
346 parameters.

347 Campbell (1974) proposed the HCF function presented in Eq. 11:

348
$$K(\theta) = K_s \left(\frac{\theta}{\theta_s} \right)^{\left(3 + \frac{2}{\lambda} \right)}$$
 (11)

349 where λ is an empirical parameter. This model only requires a single measurement of
350 unsaturated hydraulic conductivity at some moisture content to characterise the HCF. The
351 requirement for a single measurement of unsaturated hydraulic conductivity, in contrast to
352 the intensive measurement effort associated with a full laboratory characterisation, could
353 represent an efficient option for practitioners. We therefore also proposed to fit and evaluate
354 a simplified single-segment model (Eq. 12).

355
$$K(\theta) = 10^{a \cdot \theta + b}$$
 (12)

356 where a and b are empirical parameters.

357 Equations 8-10 require suitable values for the intercepts θ_1 and θ_2 to be identified. These
358 were defined based on the laboratory data. Similarly, the most suitable single-point
359 measurement to define Equation 12, was also identified based on the newly-collected
360 laboratory data.

361 **2.4 Model implementation**

362 The widely used HYDRUS 1D model could not be utilised here, as it does not support the use
363 of user-defined HCFs. Instead, the Richards Equation was solved in MATLAB (R2017b) using
364 the internal PDE (Partial Differential Equation) solver by discretising the depth of substrate
365 into 101 node points. The Richards Equation model was run at 1-minute time steps. A fuller
366 explanation of the model implementation is provided in Supplementary Material B, where it
367 is also demonstrated that the in-house model is capable of accurately reproducing the output
368 from HYDRUS 1D.

369 **2.4.1 SWRC and HCF parameters**

370 The SWRC and HCF fitting and parameter determination were performed using the SWRC Fit
371 software (Seki, 2010). The saturated hydraulic conductivity used within the HCFs was
372 determined by the FLL tests (Table 1). Initial simulations were conducted with the Durner-
373 Mualem Equation (Eqs. 4-7).

374 For further investigations, new HCFs (Eqs. 8-10 and Eq. 12) were used. Parameter values for
375 these equations were determined from the laboratory HCF data.

376 **Table 1.**

377 **2.4.2 Boundary and initial conditions**

378 For each design storm, the upper boundary was set as a Neumann condition in which the
379 surface flux equals the rainfall input R (Eq.13). Following the approach adopted in Yio et al.
380 (2013), the runoff collected from the control tests was used as rainfall input to the model. The
381 initial condition was set to be a constant hydraulic head. The moisture content at the depth

382 of the lower moisture probe was set to the measured value, and the suction head for this
383 point was calculated from the fitted SWRC (the measured moisture content and
384 corresponding suction head are listed in Table C.1 of Supplementary Material C). The suction
385 heads for the rest of the vertical profile were calculated according to Eq. 14. Following Peng
386 et al. (2019), the lower boundary was modelled as a constant hydraulic head boundary, and
387 the constant head was equivalent to the suction head of the lowest point at field capacity
388 (the initial condition before design storms were applied).

$$389 \quad K(h) \left(\frac{\partial h}{\partial z} - 1 \right) = R \quad (13)$$

390 where R is the net rainfall (cm/min) and all the symbols are as defined before.

$$391 \quad h_i = h_p - Z_i + H_p \quad (14)$$

392 where h_i (cm) is the suction head at point i and Z_i (cm) is the elevation of point i. The upper
393 layer of the substrate was assigned a value of $i = 1$. The reference level of elevation (i.e. $Z =$
394 0.0 cm) is at the bottom of the substrate, h_p is the suction head measured at the lowest probe
395 (Table C.1, Supplementary Material C) and H_p is the elevation of the lowest moisture probe
396 (P1, Fig. 2).

397 **2.5 Model evaluation**

398 The SWRC Fit software (Seki, 2010) was used to determine the parameters for the Durner and
399 van Genuchten models. The software uses R^2 to assess the goodness of fit of the models to
400 the measured SWRC data. For reference, the adjusted R^2 was also calculated from the R^2 for
401 the fitted curves. A value of R^2 or adjusted R^2 equals one corresponds to a perfect fit.

402 The root of the mean square error (RMSE) (Eq.15), was selected to assess the goodness of fit
403 for the HCFs. RMSE yields a value higher than zero, and a smaller value of RMSE indicates a

404 better prediction. The RMSE metric was also used in Liu and Fassman-Beck. (2018) to evaluate
 405 the goodness of fit of the Durner-Mualem model of unsaturated hydraulic conductivity for
 406 green roof substrates.

$$407 \quad RMSE = \sqrt{\frac{1}{N} \sum_{i=1}^N (K_m - K_p)^2} \quad (15)$$

408 where N is the number of measured data points, K_m is the measured hydraulic conductivity
 409 and K_p is the predicted hydraulic conductivity.

410 Sonnenwald et al. (2014) demonstrated that the R_t^2 (Young et al., 1980) (Eq. 16) provided a
 411 robust and generically applicable indicator of model performance for temporally-varying
 412 data. At the same time, the Nash-Sutcliffe Model Efficiency index (NSME) (Eq. 17) is routinely
 413 applied to assess model performance in hydrology (Nash and Sutcliffe, 1970). Therefore, both
 414 R_t^2 and NSME were used to evaluate the goodness-of-fit of the modelled runoff and moisture
 415 content profiles. A value of R_t^2 or NSME equal to one corresponds to a perfect match of
 416 modelled data to the observed data.

$$417 \quad R_t^2 = 1 - \frac{\sum_{i=1}^T (q_o - q_m)^2}{\sum_{i=1}^T (q_o)^2} \quad (16)$$

$$418 \quad NSME = 1 - \frac{\sum_{i=1}^T (q_o - q_m)^2}{\sum_{i=1}^T (q_o - q_{mean})^2} \quad (17)$$

419 where T is the total number of observed data, q_o is the observed runoff/moisture content
 420 data, q_m is the measured runoff/moisture content data and q_{mean} is the mean value of the
 421 observed data.

422 The R_t^2 and NSME values for all the modelled runoff and moisture content profiles can be
 423 found in Supplementary Material C.

424 **3 Results and Discussion**

425 **3.1 Substrate characteristics**

426 Table 1 lists the results of the FLL tests for the four substrates. SCS has the highest
427 permeability, suggesting that it may exhibit the worst detention effects during storm events.
428 However, the static parameters measured by FLL methods have limited relevance to the
429 dynamic behaviour of substrate moisture during storm events. It is also the case that the
430 permeability (saturated hydraulic conductivity) significantly overestimates the hydraulic
431 conductivity experienced in actual, unsaturated, conditions.

432 Particle Size Distributions (PSDs) for the four substrates are shown in Fig. 3(a). All the
433 substrates are FLL compliant. NSM was designed to contain more fine particles and the PSD
434 confirms this to be the case. The PSDs for HLS and SCS show differences in the percentages of
435 large particles; SCS contains a higher proportion of particles larger than 1 mm. The particles
436 in MCS are more evenly distributed, but it contains a slightly higher percentage of particles
437 larger than 10 mm. The photographs of the four substrates in Fig. 1 are consistent with the
438 PSD results shown in Fig. 3(a).

439 **Fig. 3.**

440 **3.2 Soil Water Release Curve (SWRC)**

441 Fig. 3(b) presents the measured points on the SWRC for the four substrates. It should be noted
442 that no pressure extractor data was obtained for NSM. However, as stated above, data
443 corresponding to high suction heads is not considered to be particularly critical for green roof
444 detention modelling. The results were plotted with error bars (\pm to the average values of three
445 tests). The results for the three replications confirm that little variation was present in the

446 SWRCs. The amount of water retained in the substrate at low suction heads (i.e. 0 cm to
447 100 cm) depends mainly on capillary effects and the pore size distribution. However, at high
448 suction heads, the substrate retains water due to adsorption, so it is influenced by the texture
449 and the specific surface of the substrate (Hillel et al., 1998). HLS showed greater water
450 retention than the other three substrates over the full range of suction heads; this may
451 indicate that it contains greater clay content. Compared with MCS and SCS, both HLS and NSM
452 exhibited a more gradual decrease in wetness with an increase in the suction head; this
453 suggests that a more uniform particle size distribution is present in HLS and NSM, which is
454 consistent with the particle size distributions presented in Fig. 3 (a). For MCS and SCS, as most
455 of the pores are large in these substrates, once these large pores are emptied (at suction
456 head > 20 cm), only a small amount of water remains.

457 Table 2 lists the calibrated parameters for the van Genuchten and Durner models for the
458 SWRC. With all R^2 and adjusted R^2 values for the Durner model higher than for van Genuchten
459 (with mean $R^2=0.997$, adjusted $R^2=0.991$ for Durner model and mean $R^2=0.989$, adjusted
460 $R^2=0.943$ for van Genuchten model), it is concluded that the Durner model provides a better
461 fit to the measured SWRC for the four substrates. The same observation was also reported in
462 Liu and Fassman-Beck (2018). Fig. 3(b) also shows the fitted SWRCs for the four substrates
463 using van Genuchten (Eq. 2) and Durner (Eq. 4) models. The MCS and SCS substrates exhibit
464 significant dual porosity characteristics, indicated by the occurrence of inflection points (0.23
465 v/v for MCS and 0.25 v/v for SCS) where the slope of the SWRC experiences a sudden change.
466 For these substrates, the van Genuchten model fails to fit the measured points. On the other
467 hand, the van Genuchten and Durner models show little difference for the HLS and NSM
468 ($R^2=0.988$ versus $R^2=0.995$ for HLS and $R^2=0.996$ versus $R^2=0.999$ for NSM). The calibrated

469 parameters listed in Table 2 for the Durner model were used as input into the Richards
470 Equation to regenerate the runoff and moisture content profiles in Section 3.6.

471 **Table 2.**

472 Field capacity is an imprecise term, usually defined in an approximate sense as the volume
473 fraction of water retained by a freely draining soil profile after the initially rapid stage of
474 internal drainage. For green roof substrates, the FLL MWHC measured in the laboratory
475 provides a practical indication of the substrate's operational field capacity.

476 Different physical definitions of field capacity can be found in the soil science and agronomy
477 literature, generally falling in the range of suction heads from 6 to 33 kPa (61 to 337 cm).
478 Many factors influence field capacity, including the texture, structure and organic matter
479 content in the soil (Hillel, 1971; Kirkham, 2004). In their detailed analysis of soil moisture
480 behaviour in green roof substrates, Fassman and Simcock (2012) adopted the value of 10 kPa
481 (approximately 100 cm) (based on the estimate provided by Hillel, 1971). However, Kirkham
482 (2004) suggests that the matric potential associated with field capacity should be measured
483 for each different soil/substrate.

484 By linking the observed FLL MWHC values for the specific substrates considered here with
485 their corresponding SWRC characteristics, it is possible to identify a suitable physical
486 definition for field capacity. It may be seen that the MWHC values for these substrates (31-
487 38%, see Table 1) are all significantly higher than the SWRC values associated with a suction
488 head of 100 cm (around 23-28%, Figure 3(b)). Indeed, the suction head associated with the
489 MWHC values is approximately 6-10 cm. This suggests that it may be appropriate to use a
490 suction head of 6-10 cm rather than 100 cm to identify nominal field capacity for green roof
491 substrates.

492 3.3 Hydraulic Conductivity Function (HCF)

493 Fig. 4 presents the measured hydraulic conductivity data for the four green roof substrates.
494 The saturated hydraulic conductivity (the first data point on the HCF) was determined by the
495 FLL tests (Table 1), and the corresponding moisture content is the porosity determined in
496 Section 3.1. The hydraulic conductivities were estimated using steady state and transient
497 techniques; within the transient technique, hydraulic conductivity was determined during
498 drainage and evaporation. However, the tensiometers failed to capture the rapid change in
499 the suction head in SCS, so no data was measured during the drainage process for SCS. It
500 should be noted that the characterisations of HCF at the high moisture content (i.e. HCF
501 determined by steady state techniques) are more critical for detention modelling.

502 Significant variations between the two repeat tests are evident. This reflects the
503 heterogeneous nature of green roof substrates. In addition, the unsaturated hydraulic
504 conductivity is a property that is very sensitive to the pore size distribution (Liu and Fassman-
505 Beck, 2018; Masch and Denny, 1966); differences in test column preparation could result in
506 different pore size distributions and therefore in differing HCFs.

507 Fig. 4 also compares the Durner-Mualem model with the measured data. Consistent with Liu
508 and Fassman-Beck (2018), the results indicate that the Durner-Mualem model is not suitable
509 to represent the HCF for green roof substrates (with mean RMSE=0.113, Table 3). The fit for
510 HLS is particularly poor, underestimating unsaturated hydraulic conductivity by around two
511 orders of magnitude at higher moisture contents (e.g. 9.67×10^{-5} cm/min was estimated by
512 the Durner-Mualem compared with a measured value of 0.015 cm/min at 0.3 v/v).

513 Given the poor fit of the Durner-Mualem model, an alternative approach to estimating a
514 continuous HCF from the laboratory data was required. Whilst some scatter in the data is

515 evident, the laboratory measurements typically exhibit one or two changes in slope. This led
516 to a proposal to fit a three-segment curve (Eqs. 8-10) to the measured data. It was noted that
517 the two intercepts typically occurred at moisture contents associated with two specific
518 suction heads, 6 and 100 cm (Fig. 4). As indicated earlier, these two values are associated with
519 the MWHC (or practical field capacity) of these green roof substrates and with nominal field
520 capacity in conventional soils respectively. Vertical lines indicating the corresponding
521 moisture contents from the SWRCs are included in Figure 4 for reference. The use of a
522 piecewise linear function to characterise the HCF is not novel. Poulsen et al. (2002) have
523 shown that three-region models can be fitted to a wide range of natural soils. Furthermore,
524 they assigned similar intercepts (at suction heads of 10 and 350 cm), suggesting that these
525 intercept values delineate independent functions associated with the macropore, mesopore
526 and micropore regions.

527 **Fig. 4.**

528 The mean RMSE for the HCF decreased from 0.113 to 0.060 when the three-segment curves
529 were adopted (Table 3). As two infiltration column tests were conducted, two three-segment
530 curves were derived from the measured data for each substrate. The three-segment curves
531 presented in Fig. 4 are the average of the two tests. The influence of the Durner-Mualem and
532 the three-segment HCF models on the detention model results will be discussed in Section
533 3.6.

534 **Table 3.**

535 3.4 Detention performance

536 Fig. 5 presents the runoff profiles for the four substrates in response to four design storms.
537 The left column presents the runoff profiles for the 100 mm substrates, and the right column
538 corresponds to the 200 mm substrates. The runoff from the no substrate test confirms that
539 the apparatus is capable of providing the desired rainfall rates.

540 In the shallow 100 mm substrates, as the detention tests started after initial wetting, with the
541 substrate nominally at field capacity (Table C.1, Supplementary Material C), none of the
542 substrates showed a significant delay in the time to start of runoff. Interestingly, HLS and NSM
543 showed similar responses to the storms and MCS performed similarly to SCS. In Design Storm
544 1 it may be seen that runoff from the HLS and NSM substrates equilibrates with the rainfall
545 relatively quickly (around 7 minutes). In contrast, runoff from the MCS and SCS substrates
546 shows much greater detention (i.e. peak runoff is reduced by 10.7% compared with peak
547 rainfall), and equilibrium is not reached before the end of the 30-minute rainfall.

548 The detention effects are more significant, and the differences between substrates are more
549 obvious in a deeper system (i.e. 200 mm substrate). In response to a low intensity storm event
550 (Design Storm 1), MCS demonstrated the highest detention potential, it reduced the peak
551 rainfall by $57.83\% \pm 6.33\%$ and extended the duration of runoff to beyond 120 minutes. In
552 contrast, the HLS showed the lowest detention potential since it only reduced the peak
553 rainfall by $9.67\% \pm 1.89\%$ and extended the duration of runoff to 60 minutes. Within the
554 200 mm substrates, in response to a peaked storm (Design Storm 4), HLS showed the lowest
555 reduction in peak runoff ($25.66\% \pm 0.70\%$) and MCS showed the highest reduction
556 ($46.65\% \pm 4.87\%$); HLS delayed the time to start of runoff by about 5 minutes, MCS delayed it
557 by about 15 minutes. There are no significant differences between SCS and NSM in response

558 to Design Storms 2 and 3, SCS has a slightly lower peak runoff reduction in response to Design
559 Storm 1 ($21.87\% \pm 3.04\%$).

560 Overall, HLS exhibits the worst detention performance, and MCS shows the best; detention
561 performance is consistently improved by increasing the depth of the substrate. The
562 observations here are consistent with the finding in Stovin et al. (2015) and Yio et al. (2013).

563 **Fig. 5.**

564 **3.5 Moisture content behaviour during storms**

565 Moisture content responses for all four substrates for all four design storms are shown in Figs.
566 C.4, C.5, C.6 and C.7, Supplementary Material C. As the response to all four design storms is
567 similar, Fig. 6 only presents the moisture content data from the four substrates for Design
568 Storm 3. It should be noted that the secondary y-axis range is not consistent between sub-
569 plots. The moisture content responses in the substrates showed significant differences
570 between substrates and depths.

571 The moisture content profiles in the 100 mm substrates confirm that the moisture content
572 increases simultaneously with the rainfall, and the moisture content returns to its initial value
573 once the rainfall stops. The moisture content in the 100 mm SCS experienced the most
574 dramatic change during the storm: it increased about 0.03 v/v at the peak. In contrast, HLS
575 showed the smallest increase, around 0.015 v/v.

576 The two moisture probes in the 200 mm substrates make it possible to investigate the vertical
577 moisture content profiles during storms. Fig. 6 shows the measured moisture content data at
578 the top and bottom of the substrates. Vertical gradients in moisture content were clearly
579 present within the substrates. The top substrate was always wetter than the bottom substrate,

580 and the top substrate always responded faster to the storm than the bottom substrate. The
581 vertical gradient is significant in HLS and NSM; the moisture content at the bottom of these
582 two substrates showed almost no increase (about 0.001 v/v increase for HLS and less than
583 0.0005 v/v increase for NSM at the peaks) during the storm. The greater gradient shown in
584 HLS and NSM implies that they had a lower unsaturated hydraulic conductivity than MCS or
585 SCS. Temporal variations in vertical substrate moisture content profiles were presented for
586 shallow external green roof test beds in Peng et al. (2019). A greater peak to peak vertical
587 moisture content gradient was observed in Peng et al. (2019) (2.4 v/v/m versus 0.8 v/v/m),
588 and the gradient was also typically reversed. It has been suggested that the presence of
589 vegetation and substrate consolidation over time may contribute to the development of
590 vertical gradients observed in external test beds (Berretta et al., 2014), but it is also
591 acknowledged that other factors - including uncertainties associated with the calibration of
592 moisture content probes and their siting within heterogeneous substrates - also impact on
593 the absolute measured values. Acknowledging these uncertainties in absolute measured
594 values, further discussion on vertical profiles is considered to be beyond the scope of the
595 current paper, and the moisture content profiles presented in Fig. 6 will subsequently be
596 presented as values relative to the local initial moisture content.

597 As the detention tests started from field capacity, runoff occurs immediately after the rainfall,
598 and a wetting front was not present in every substrate. The 200 mm MCS shows some
599 evidence of a wetting front, with the response in the lower substrate layer occurring about 8
600 minutes later than the top.

601 Fig. 6 also shows the runoff response to the storm. Liu and Fassman-Beck (2017) observed
602 that preferential flow paths developed in the substrate during the storm when the substrate

603 was initially relatively dry. However, based on the runoff and vertical moisture content
604 profiles measured for the 200 mm substrates, during the storms in this study, there is no
605 strong evidence for the occurrence of preferential flow within green roof substrates. The
606 runoff increases simultaneously with the rise in bottom moisture content, and in no case was
607 runoff generated before the bottom moisture started to increase.

608 The measured moisture contents at the start and end of the detention tests are generally
609 closer to the FLL MWHC values (e.g. 0.34 v/v was the measured value for the 200 mm NSM
610 and 0.36 v/v for the FLL MWHC) than the SWRC values corresponding to 100 cm suction head
611 (Table 1, Fig. 6 and Table C.1, Fig. C.4 Supplementary Material C), providing further indication
612 that field capacity in these substrates may correspond to a lower suction head than is the case
613 for conventional soils. Any differences between the absolute values reported here, and the
614 MWHC values reported in Table 1 are likely to result from slight discrepancies in the moisture
615 probe calibrations and/or the use of different sub-samples for the specific tests.

616 **Fig. 6.**

617 **3.6 Model validation**

618 The HCF is required as an input into the Richards Equation. Two HCF models (Durner-Mualem
619 and the three-segment laboratory curve, Fig. 4) were applied in the Richards Equation model
620 to generate the runoff and moisture content profiles for the 100 mm and 200 mm substrates
621 in response to the four design storms. The coefficients of determination (R_t^2) and the Nash-
622 Sutcliffe Model Efficiency (NSME) were calculated for the modelled runoff using the two HCF
623 models. As the three-segment curve was derived from measured HCF data points, it provides
624 a better representation of the HCF and, consequently, led to improved model performance

625 (mean R_t^2 of 0.754 and NSME of 0.725) compared with Durner-Mualem HCF (mean R_t^2 of
626 0.409 and NSME of 0.268) (Tables C.3, C.4 and Figs. C.3, C.4, Supplementary Material C).

627 The modelled runoff profiles using the two HCF models for all the substrates and depths are
628 similar (Figs. C.8 and C.9, Supplementary Material C). However, the differences between
629 models are more significant in deeper substrate in response to heavier rainfall. As a
630 consequence, the 200 mm substrates and Design Storms 3 and 4 were selected for further
631 discussion. Fig. 7 compares modelled and measured runoff profiles from the 200 mm
632 substrates in response to Design Storms 3 and 4. The two HCF models led to different
633 predictions of runoff profiles and the performance of the models varied across substrates.

634 As both the Durner-Mualem model and the three-segment curve provided a good agreement
635 with the measured HCF data points (Fig. 4) for MCS, they both led to reasonable predictions
636 of runoff profiles for MCS (Fig. 7). Slight differences were present in the modelled runoff
637 profiles, with the Durner-Mualem model delaying the time to start of runoff (10 minutes) by
638 about 5 minutes compared with the three-segment curve (5 minutes). The three-segment
639 curve gives a peak runoff rate (0.797 cm/min) about 100% higher than the Durner-Mualem
640 model (0.367 cm/min) in response to Design Storm 4. Comparing the modelled runoff profiles
641 with measured profiles, the three-segment curve tends to overestimate the peak runoff rate
642 and the Durner-Mualem model is more likely to delay the time of peak runoff and the time to
643 start of runoff.

644 The influence of the two different HCFs on modelled runoff is particularly striking for HLS (Fig.
645 7(c) and 7(d)). The detention effects are significantly overestimated by the Durner-Mualem
646 model. The time to start of runoff is delayed by up to 25 minutes in response to Design Storm
647 3; in the case of Design Storm 4, the peak runoff rate was underestimated by 88%. The model

648 results are significantly improved when using the three-segment curve. The time to start of
649 runoff is modelled well by the three-segment curve and the rising and falling limbs are
650 modelled reasonably. However, the three-segment curve slightly underestimates (13.3%) the
651 peak runoff rate in Design Storm 4. It is not surprising that the two models showed noticeable
652 differences; HCF influences the model results and the two HCF models differed significantly
653 for this substrate (Fig. 4).

654 SCS shows further interesting results (Fig. 7(e) and 7(f)). The two HCF models generated
655 different runoff profiles. However, unlike HLS, the model results are worse when using the
656 three-segment curve, which overestimated the detention effects. It is possible that due to the
657 heterogeneous nature of the substrates, neither of the infiltration column tests for the HCF
658 characterisations was a good representation of the fresh sample of SCS substrate utilised in
659 the detention tests.

660 The model results for NSM (Fig. 7(g) and 7(h)) are consistent with the results of HLS.
661 Significant differences are present in the results using the two HCF models and the model
662 results are improved when using the three-segment curve.

663 Liu and Fassman-Beck (2017) also obtained poor model predictions when using the Durner-
664 Mualem HCF. They attributed this to preferential flow, and demonstrated that improved
665 predictions could be obtained when a mobile-immobile dual porosity model was applied. In
666 contrast, in this study, the model results were improved by using a HCF that better represents
667 the measured unsaturated hydraulic conductivity data, without increasing the complexity of
668 the unsaturated flow model (Richards Equation).

669 **Fig. 7.**

670 Further validation is provided by the substrate moisture content variations during the storm
671 events. Fig. 8 compares the modelled and measured vertical moisture content profiles in
672 response to Design Storm 3. However, the model results for all four design storms are similar
673 (see Figs. C.10 and C.11, Supplementary Material C). The moisture content at any depth
674 returns to its initial moisture content when the rainfall stops (Fig. 6). Therefore, to highlight
675 the dynamics of moisture changes in the substrate, the moisture content presented in Fig. 8
676 is relative to initial moisture content. Consistent with the modelled runoff profiles, the
677 differences in modelled vertical moisture content profiles between the two models are minor
678 where the two models gave close predictions for HCFs (the case for MCS) (Fig. 8(a)), and the
679 model gives reasonable predictions of vertical moisture content profiles when the HCF is
680 correctly modelled. The Durner-Mualem model tends to overestimate the vertical gradient in
681 the substrate (it overestimated the top moisture content and underestimated the bottom
682 moisture content), and the three-segment curve leads to better overall model performance
683 compared with the Durner-Mualem model (Tables C.5 and C.6, Fig. C.11, Supplementary
684 Material C). The differences between modelled (three-segment curve) and measured
685 moisture contents are minor for the cases of MCS and NSM. The worst case was for SCS,
686 where the three-segment curve gives a peak moisture content value at the top of the
687 substrate that is 0.05 v/v higher than measured. However, it should be noted that for the case
688 of SCS, any difference between the measured and modelled moisture content could be due
689 to the uncertainties associated with subsampling.

690 Overall, the results indicate that the Richards Equation is capable of modelling the detention
691 effects in green roof substrates if the HCF is correctly represented. Both the runoff and
692 moisture content profiles of the substrates during the storms can be reasonably modelled.
693 The detention model comparisons highlight the importance – in this context – of correctly

694 characterising unsaturated hydraulic conductivities in the ‘wet’ range between field capacity
695 and saturation.

696 **Fig. 8.**

697 **3.7 A simplified model for HCF**

698 Modelling green roof substrate detention using the Richards Equation requires several input
699 parameters. Previous sections have highlighted the importance of having appropriate HCF
700 data to accurately model detention effects within green roof substrates. However, the
701 method described in Section 2.2.3 for characterising the HCF requires intensive measurement
702 of moisture content, suction heads and infiltration rates, which is complex and time-
703 consuming. In this section, a simplified approach is proposed, whereby only two data points
704 on the HCF are required to derive the HCF.

705 The saturated hydraulic conductivity (measured using the FLL method) and the averaged
706 moisture content of the two tests corresponding to a hydraulic conductivity of 0.1 cm/min
707 were selected to define the HCF using Eq. 12. The justification for choosing 0.1 cm/min is that
708 it represents a moderate infiltration rate which can be easily achieved by the apparatus, and
709 the time for the substrate to reach equilibrium under this flow rate is relatively short. In
710 addition, this value also typically falls within the range between field capacity and saturation,
711 which is the range of interest for detention modelling.

712 Fig. 9 shows the derived HCFs for HLS and NSM using the simplified approach. Compared with
713 the Durner-Mualem model, the simplified laboratory curve shows a better agreement with
714 the measured HCF data points for high moisture content (i.e. above field capacity), than for
715 low moisture content. However, during storm events, the moisture content in the substrate

716 does not fall below field capacity (Fig. 6), and the HCF at high moisture content is more
717 relevant.

718 **Fig. 9**

719 Compared with the model results using the Durner-Mualem approach, the simplified
720 laboratory curve provides a much better overall estimate of green roof detention
721 performance (with mean R_t^2 of 0.629 versus 0.409 and NSME of 0.456 versus 0.268) (Figs. C.3
722 and C.4, Supplementary Material C). However, the simplified laboratory curve has slightly
723 worse performance than the three-segment curve (with mean R_t^2 of 0.629 versus 0.754 and
724 NSME of 0.456 versus 0.725) (Figs. C.3 and C.4, Supplementary Material C).

725 The model results for 200 mm HLS and NSM in response to Design Storm 3 are presented in
726 Fig. 10 to illustrate typical model performance. Model results using the simplified laboratory
727 curve for the other substrates are similarly good. HLS and NSM are the two cases where the
728 Durner-Mualem model significantly underestimated the HCF and resulted in a poor
729 performance of the model in regenerating the runoff profiles. However, the model results
730 improved significantly when the simplified laboratory curve was utilized; the R_t^2 increased to
731 above 0.93 and the NSME increased to above 0.92 in both cases. The peak runoff rates were
732 estimated well and the rising and falling limbs were modelled reasonably.

733 **Fig. 10.**

734 The combination of results provides some support for the application of this simplified
735 approach to determining the HCF. As the simplified laboratory curve can provide reasonable
736 predictions of runoff profiles, the HCF characterisation can be reduced to the measurement
737 of just two data points: the saturated hydraulic conductivity and the steady moisture content
738 under an infiltration rate of 0.1 cm/min. Although the model results based on the simplified

739 laboratory curve are not as good as those based on the three-segment curve, the simplified
740 approach reduces the complexity and time (from 5 weeks to one day) required for HCF
741 measurements, which offers considerable benefits in terms of practical application.

742 **4 Conclusions**

743 With the purpose of building a better understanding of hydraulic conductivity within green
744 roof substrates during storm events, a series of physical characterisation experiments was
745 conducted on four representative green roof substrates.

746 The SWRC data for the four green roof substrates confirmed that the Durner model correctly
747 represents the water release characteristics of the substrates. However, the comparison
748 between measured and estimated hydraulic conductivity showed that the conventional
749 approach for estimating hydraulic conductivity (Durner-Mualem) failed to represent the HCF
750 for green roof substrates accurately. In addition, variations observed in the HCF experiments
751 highlighted the heterogeneous nature of green roof substrates.

752 Comparisons between the SWRCs and actual moisture contents observed when the
753 substrates were judged to have drained to field capacity suggest that moisture content
754 measured at 6-10 cm suction head may provide a better practical estimate of field capacity in
755 the brick-based green roof substrates than the 100 cm value typically assumed for natural
756 soils.

757 The runoff and moisture content profiles measured for the substrates during simulated storm
758 events clearly demonstrated different substrate responses. Consistent with the findings of
759 Stovin et al. (2015), HLS demonstrated the poorest detention performance. The measured
760 vertical moisture content profiles indicated that vertical gradients exist within the substrate

761 and the change in moisture content in response to a storm is more rapid at the top of the
762 substrate.

763 Comparisons between measured and modelled runoff profiles have confirmed that Richards
764 Equation based models are capable of modelling detention effects within green roof
765 substrates. The results also showed that the moisture content profiles can be accurately
766 regenerated by Richards Equation based models if the HCF is correctly represented. HCF
767 curves derived from measured HCF data points result in better performance than the
768 conventional Durner-Mualem approach.

769 A simplified HCF proposed here provides reasonable estimations of runoff profiles. This
770 approach simplifies the procedures and saves time for HCF determination, which has practical
771 implications for the application of the Richards Equation in modelling the detention effects
772 due to green roof substrates.

773 **5 Acknowledgements**

774 Zhangjie Peng is supported by the University of Sheffield, Faculty of Engineering Doctoral
775 Academy Award. The authors would like to thank Jörg Werdin for the measurement of Soil
776 Water Release Curve with the pressure extractor; the authors would also like to thank Martin
777 Taylor, Mark Foster, Paul Osborne and Kieran Nash for their contributions in establishing the
778 experimental apparatus.

779 **6 References**

- 780 ASTM. 2010. "Standard test method for measurement of hydraulic conductivity of
781 unsaturated soils." ASTM D7664-10, West Conshohocken, PA.
782 <https://doi.org/10.1520/D7664>
- 783 Berretta, C., Poë, S., Stovin, V., 2014. Reprint of "Moisture content behaviour in extensive
784 green roofs during dry periods: The influence of vegetation and substrate
785 characteristics." *J. Hydrol.* 516, 37–49. <https://doi.org/10.1016/j.jhydrol.2014.04.001>
- 786 Bouzouidja, R., Séré, G., Claverie, R., Ouvrard, S., Nuttens, L., Lacroix, D., 2018. Green roof
787 aging: Quantifying the impact of substrate evolution on hydraulic performances at the
788 lab-scale. *J. Hydrol.* 564, 416–423. <https://doi.org/10.1016/j.jhydrol.2018.07.032>
- 789 Brunetti, G., Šimůnek, J., Piro, P., 2016. A Comprehensive Analysis of the Variably Saturated
790 Hydraulic Behavior of a Green Roof in a Mediterranean Climate. *Vadose Zo. J.* 15, 0.
791 <https://doi.org/10.2136/vzj2016.04.0032>
- 792 Campbell, G.S., 1974. A simple method for determining unsaturated conductivity from
793 moisture retention data. *Soil Sci.* 117, 311–314.
- 794 Carter, M.R., Gregorich, E.G., 2007. *Soil Sampling and Methods of Analysis, Second Edition,*
795 2nd Editio. ed. CRC Press, Boca Raton. <https://doi.org/10.1201/9781420005271>
- 796 Castiglia Feitosa, R., Wilkinson, S., 2016. Modelling green roof stormwater response for
797 different soil depths. *Landsc. Urban Plan.* 153, 170–179.
798 <https://doi.org/10.1016/J.LANDURBPLAN.2016.05.007>
- 799 De-Ville, S., Menon, M., Jia, X., Reed, G., Stovin, V., 2017. The impact of green roof ageing on
800 substrate characteristics and hydrological performance. *J. Hydrol.* 547, 332–344.

801 <https://doi.org/10.1016/j.jhydrol.2017.02.006>

802 Durner, W., 1994. Hydraulic conductivity estimation for soils with heterogeneous pore
803 structure. *Water Resour. Res.* 30, 211–223. <https://doi.org/10.1029/93WR02676>

804 Fassman-Beck, E., Voyde, E., Simcock, R., Hong, Y.S., 2013. 4 Living roofs in 3 locations: Does
805 configuration affect runoff mitigation? *J. Hydrol.* 490, 11–20.
806 <https://doi.org/10.1016/J.JHYDROL.2013.03.004>

807 Fassman, E., Simcock, R., 2012. Moisture Measurements as Performance Criteria for Extensive
808 Living Roof Substrates. *J. Environ. Eng.* 138, 841–851.
809 [https://doi.org/10.1061/\(ASCE\)EE.1943-7870.0000532](https://doi.org/10.1061/(ASCE)EE.1943-7870.0000532)

810 FLL, 2008. FLL (Forschungsgesellschaft Landschaftsentwicklung Landschaftsbau), (2008).
811 Guidelines for the Planning, Construction and Maintenance of Green Roofing.
812 Forschungsgesellschaft Landschaftsentwicklung Landschaftsbau e. V., Bonn, Germany.
813 119.

814 Hillel, D., 1971. *Soil and Water: Physical Principles and Processes*, Soil Science Society of
815 America Journal. Academic Press.

816 Hillel, D., Warrick, A.W., Baker, R.S., Rosenzweig, C., 1998. *Environmental soil physics*.
817 Academic Press.

818 Hilten, R.N., Lawrence, T.M., Tollner, E.W., 2008. Modeling stormwater runoff from green
819 roofs with HYDRUS-1D. *J. Hydrol.* <https://doi.org/10.1016/j.jhydrol.2008.06.010>

820 Kasmin, H., Stovin, V.R., Hathway, E.A., 2010. Towards a generic rainfall-runoff model for
821 green roofs. *Water Sci. Technol.* 62, 898. <https://doi.org/10.2166/wst.2010.352>

822 Kirkham, M.B., 2004. *Principles of Soil and Plant Water Relations*, Principles of Soil and Plant

823 Water Relations. Elsevier Inc. <https://doi.org/10.1016/B978-0-12-409751-3.X5000-2>

824 Liu, R., Fassman-Beck, E., 2018. Pore Structure and Unsaturated Hydraulic Conductivity of
825 Engineered Media for Living Roofs and Bioretention Based on Water Retention Data. J.
826 Hydrol. Eng. 23, 04017065. [https://doi.org/10.1061/\(ASCE\)HE.1943-5584.0001621](https://doi.org/10.1061/(ASCE)HE.1943-5584.0001621)

827 Liu, R., Fassman-Beck, E., 2017. Hydrologic response of engineered media in living roofs and
828 bioretention to large rainfalls: experiments and modeling. Hydrol. Process. 31, 556–572.
829 <https://doi.org/10.1002/hyp.11044>

830 Liu, R., Fassman-Beck, E., 2016. Effect of Composition on Basic Properties of Engineered
831 Media for Living Roofs and Bioretention. J. Hydrol. Eng. 21, 06016002.
832 [https://doi.org/10.1061/\(asce\)he.1943-5584.0001373](https://doi.org/10.1061/(asce)he.1943-5584.0001373)

833 Masch, F.D., Denny, K.J., 1966. Grain size distribution and its effect on the permeability of
834 unconsolidated sands. Water Resour. Res. 2, 665–677.
835 <https://doi.org/10.1029/WR002i004p00665>

836 Mualem, Y., 1976. A new model for predicting the hydraulic conductivity of unsaturated
837 porous media. Water Resour. Res. 12, 513–522.
838 <https://doi.org/10.1029/WR012i003p00513>

839 Nash, J.E., Sutcliffe, J.V., 1970. River flow forecasting through conceptual models part I — A
840 discussion of principles. J. Hydrol. 10, 282–290. [https://doi.org/10.1016/0022-](https://doi.org/10.1016/0022-1694(70)90255-6)
841 [1694\(70\)90255-6](https://doi.org/10.1016/0022-1694(70)90255-6)

842 NERC, 1975. Flood Studies Report. Natural Environment Research Council, London.

843 NERC, 1999. Flood Estimation Handbook (CD). Natural Environment Research Council,
844 London.

845 Palermo, S.A., Turco, M., Principato, F., Piro, P., 2019. Hydrological Effectiveness of an
846 Extensive Green Roof in Mediterranean Climate. *Water* 11, 1378.
847 <https://doi.org/10.3390/w11071378>

848 Palla, A., Gnecco, I., Lanza, L.G., 2012. Compared performance of a conceptual and a
849 mechanistic hydrologic models of a green roof. *Hydrol. Process.* 26, 73–84.
850 <https://doi.org/10.1002/hyp.8112>

851 Palla, A., Gnecco, I., Lanza, L.G., 2009. Unsaturated 2D modelling of subsurface water flow in
852 the coarse-grained porous matrix of a green roof. *J. Hydrol.* 379, 193–204.
853 <https://doi.org/10.1016/j.jhydrol.2009.10.008>

854 Peng, Z., Smith, C., Stovin, V., 2019. Internal fluctuations in green roof substrate moisture
855 content during storm events: Monitored data and model simulations. *J. Hydrol.* 573,
856 872–884. <https://doi.org/10.1016/j.jhydrol.2019.04.008>

857 Peng, Z., Stovin, V., 2017. Independent Validation of the SWMM Green Roof Module. *J.*
858 *Hydrol. Eng.* 22, 04017037. [https://doi.org/10.1061/\(asce\)he.1943-5584.0001558](https://doi.org/10.1061/(asce)he.1943-5584.0001558)

859 Poë, S., Stovin, V., Berretta, C., 2015. Parameters influencing the regeneration of a green
860 roof's retention capacity via evapotranspiration. *J. Hydrol.* 523, 356–367.
861 <https://doi.org/10.1016/J.JHYDROL.2015.02.002>

862 Poulsen, T.G., Moldrup, P., Iversen, B. V., Jacobsen, O.H., 2002. Three-region Campbell Model
863 for Unsaturated Hydraulic Conductivity in Undisturbed Soils. *Soil Sci. Soc. Am. J.* 66, 744–
864 752. <https://doi.org/10.2136/sssaj2002.7440>

865 Richards, L.A., 1931. Capillary conduction of liquids through porous mediums. *J. Appl. Phys.* 1,
866 318–333. <https://doi.org/10.1063/1.1745010>

867 Rossman, L.A., Huber, W.C., 2016. Storm Water Management Model Reference Manual
868 Volume III – Water Quality. United States Environ. Prot. Agency III, 235.
869 <https://doi.org/EPA/600/R-15/162> |

870 Seki, K., 2010. SWRC fit: a nonlinear fitting program with a water retention curve for soils
871 having unimodal and bimodal pore structure. *Hydrol. Earth Syst. Sci. Discuss.* 4, 407–437.
872 <https://doi.org/10.5194/hessd-4-407-2007>

873 Sims, A.W., Robinson, C.E., Smart, C.C., O’Carroll, D.M., 2019. Mechanisms controlling green
874 roof peak flow rate attenuation. *J. Hydrol.* 577, 123972.
875 <https://doi.org/10.1016/j.jhydrol.2019.123972>

876 Šimůnek, J., Šejna, M., Saito, H., Sakai, M., Genuchten, M.T. Van, 2013. The HYDRUS-1D
877 Software Package for Simulating the Movement of Water, Heat, and Multiple Solutes in
878 Variably Saturated Media, Version 4.17, HYDRUS Software Series 3, Department of
879 Environmental Sciences, University of California Riverside, Riverside, Cali 343.

880 Sonnenwald, F., Stovin, V., Guymer, I., 2014. Configuring maximum entropy deconvolution for
881 the identification of residence time distributions in solute transport applications. *J.*
882 *Hydrol. Eng.* 19, 1413–1421. [https://doi.org/10.1061/\(ASCE\)HE.1943-5584.0000929](https://doi.org/10.1061/(ASCE)HE.1943-5584.0000929)

883 Soulis, K.X., Valiantzas, J.D., Ntoulas, N., Kargas, G., Nektarios, P.A., 2017. Simulation of green
884 roof runoff under different substrate depths and vegetation covers by coupling a simple
885 conceptual and a physically based hydrological model. *J. Environ. Manage.* 200, 434–445.
886 <https://doi.org/10.1016/j.jenvman.2017.06.012>

887 Stovin, V., Poë, S., Berretta, C., 2013. A modelling study of long term green roof retention
888 performance. *J. Environ. Manage.* 131, 206–215.
889 <https://doi.org/10.1016/j.jenvman.2013.09.026>

890 Stovin, V., Poë, S., De-Ville, S., Berretta, C., 2015. The influence of substrate and vegetation
891 configuration on green roof hydrological performance. *Ecol. Eng.* 85, 159–172.
892 <https://doi.org/10.1016/j.ecoleng.2015.09.076>

893 Stovin, V., Vesuviano, G., De-Ville, S., 2017. Defining green roof detention performance.
894 *Urban Water J.* 14, 574–588. <https://doi.org/10.1080/1573062X.2015.1049279>

895 Stovin, V., Vesuviano, G., Kasmin, H., 2012. The hydrological performance of a green roof test
896 bed under UK climatic conditions. *J. Hydrol.* 414–415, 148–161.
897 <https://doi.org/10.1016/J.JHYDROL.2011.10.022>

898 van Genuchten, M.T., 1980. A Closed-form Equation for Predicting the Hydraulic Conductivity
899 of Unsaturated Soils. *Soil Sci. Soc. Am. J.* 44, 892–898.
900 <https://doi.org/10.2136/sssaj1980.03615995004400050002x>

901 Vesuviano, G., Sonnenwald, F., Stovin, V., 2014. A two-stage storage routing model for green
902 roof runoff detention. *Water Sci. Technol.* 69, 1191.
903 <https://doi.org/10.2166/wst.2013.808>

904 Voyde, E., Fassman, E., Simcock, R., 2010. Hydrology of an extensive living roof under sub-
905 tropical climate conditions in Auckland, New Zealand. *J. Hydrol.* 394, 384–395.
906 <https://doi.org/10.1016/J.JHYDROL.2010.09.013>

907 Yio, M.H.N., Stovin, V., Werdin, J., Vesuviano, G., 2013. Experimental analysis of green roof
908 substrate detention characteristics. *Water Sci. Technol.* 68, 1477–1486.
909 <https://doi.org/10.2166/wst.2013.381>

910 Young, P., Jakeman, A., McMurtrie, R., 1980. An instrumental variable method for model
911 order identification. *Automatica* 16, 281–294. <https://doi.org/10.1016/0005->

912 1098(80)90037-0

913

Table 1. Substrate physical characteristics according to FLL (2008) test methods.

Note: Marie Curie Substrate (MCS); Heather with Lavender Substrate (HLS); Sedum Carpet Substrate (SCS); New Substrate Mix (NSM).

Properties	Unit	MCS		HLS		SCS		NSM	
		Mean	St.Dev	Mean	St.Dev	Mean	St.Dev	Mean	St.Dev
Particle size<0.063 mm	%	0.00	0.00	2.72	0.25	2.64	1.33	0.00	0.00
d ₅₀	mm	3.97	0.49	5.05	0.07	7.25	0.35	2.58	0.39
Bulk density	g/cm ³	1.04	0.03	0.81	0.05	0.91	0.03	1.00	0.04
Porosity	%	55.15	0.02	55.60	0.85	53.99	0.45	48.64	0.02
Maximum water holding capacity	%	33.39	0.01	38.08	0.01	31.00	0.01	36.05	0.01
Permeability	mm/min	166.40	6.90	26.79	0.92	194.91	9.13	67.83	3.16

Table 2. Fitted Soil Water Release Curve (SWRC) parameters for the substrates.

Parameter	Durner				Parameter	van Genuchten			
	MCS	HLS	SCS	NSM		MCS	HLS	SCS	NSM
Θ_s	0.552	0.556	0.54	0.486	Θ_s	0.552	0.556	0.54	0.486
Θ_r	0.042	0	0	0	Θ_r	0	0	0	0
α_1	0.304	0.306	0.456	0.707	α	26.025	0.807	8.751	1.459
n ₁	2.82	2.255	2.182	1.708	n	1.116	1.157	1.121	1.155
α_2	5.09E-04	0.02	0.002	0.021	R ²	0.933	0.988	0.979	0.996
n ₂	1.926	1.194	1.267	1.184	Adjusted R ²	0.855	0.973	0.954	0.991
w ₁	0.622	0.378	0.528	0.462					
R ²	0.996	0.995	0.997	0.999					
Adjusted R ²	0.989	0.986	0.992	0.997					

Table 3. RMSE for the Durner-Mualem model and the Three-Segment curve.

Substrate	Test	Durner-Mualem	Three-Segment Curve
MCS	1	0.146	0.060
	2	0.121	0.132
HLS	1	0.090	0.044
	2	0.095	0.089
SCS	1	0.238	0.057
	2	0.122	0.050
NSM	1	0.032	0.018
	2	0.059	0.033
Mean	-	0.113	0.060

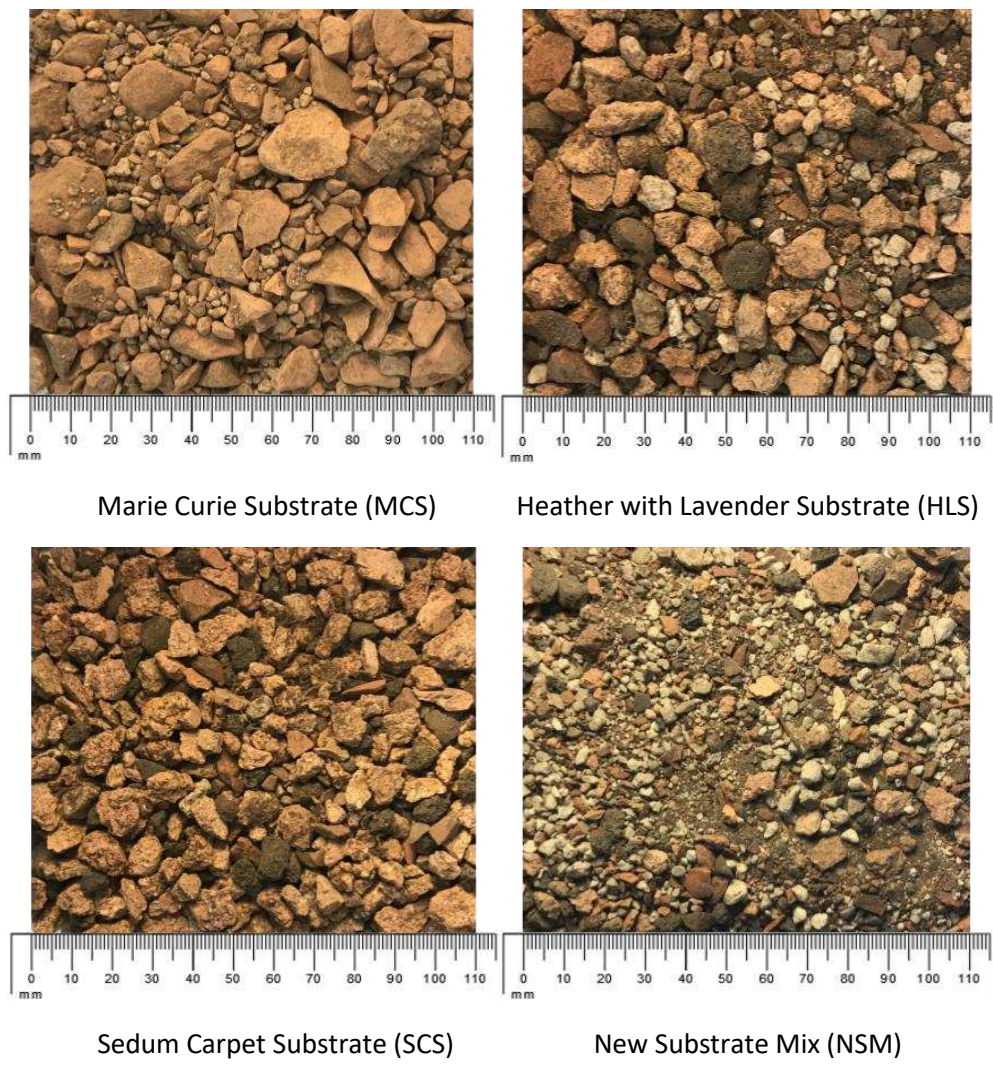


Fig. 1. Photographs of the four trial substrates.

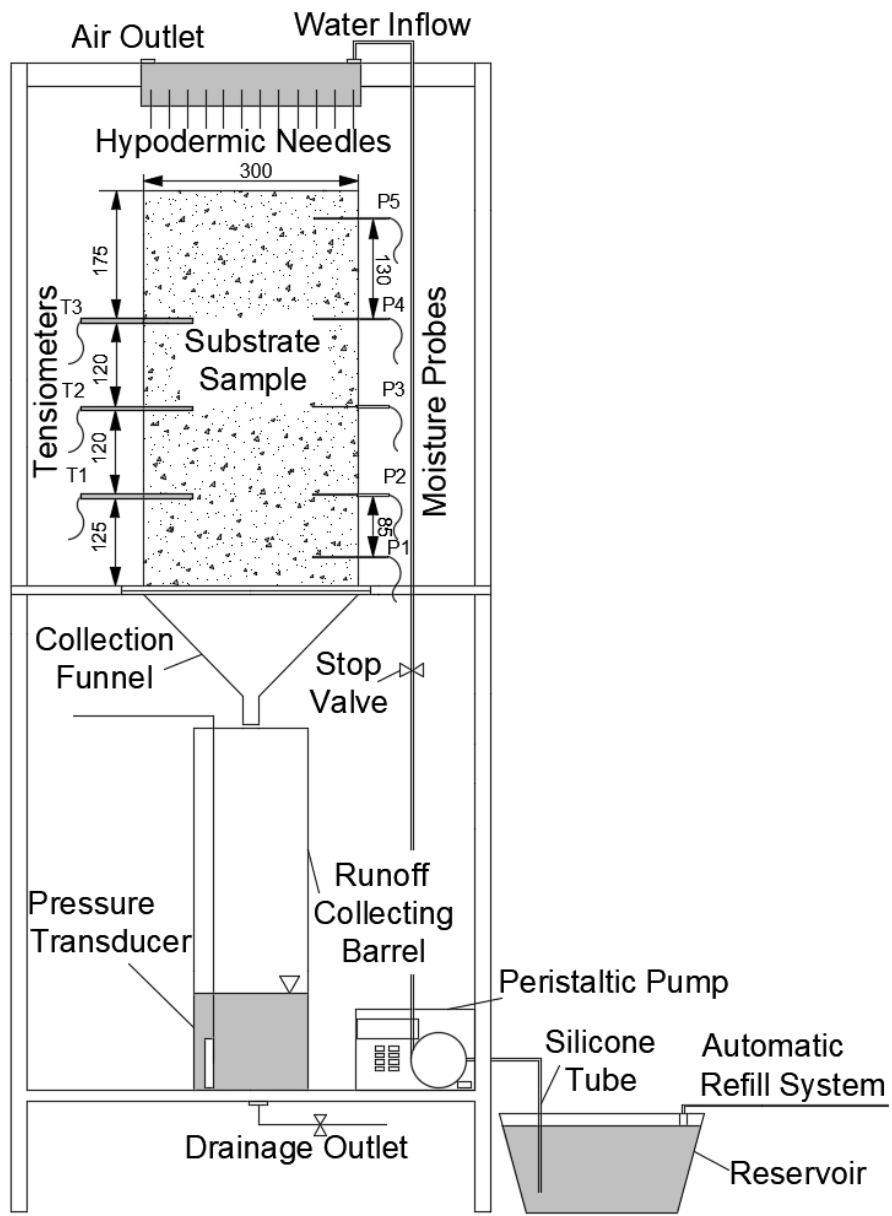


Fig. 2. Experimental set up for the measurement of hydraulic conductivity, runoff and vertical moisture content profiles (P1, P2, P3, P4, P5 are the moisture probes and T1, T2, T3 are the tensiometers; all dimensions in mm).

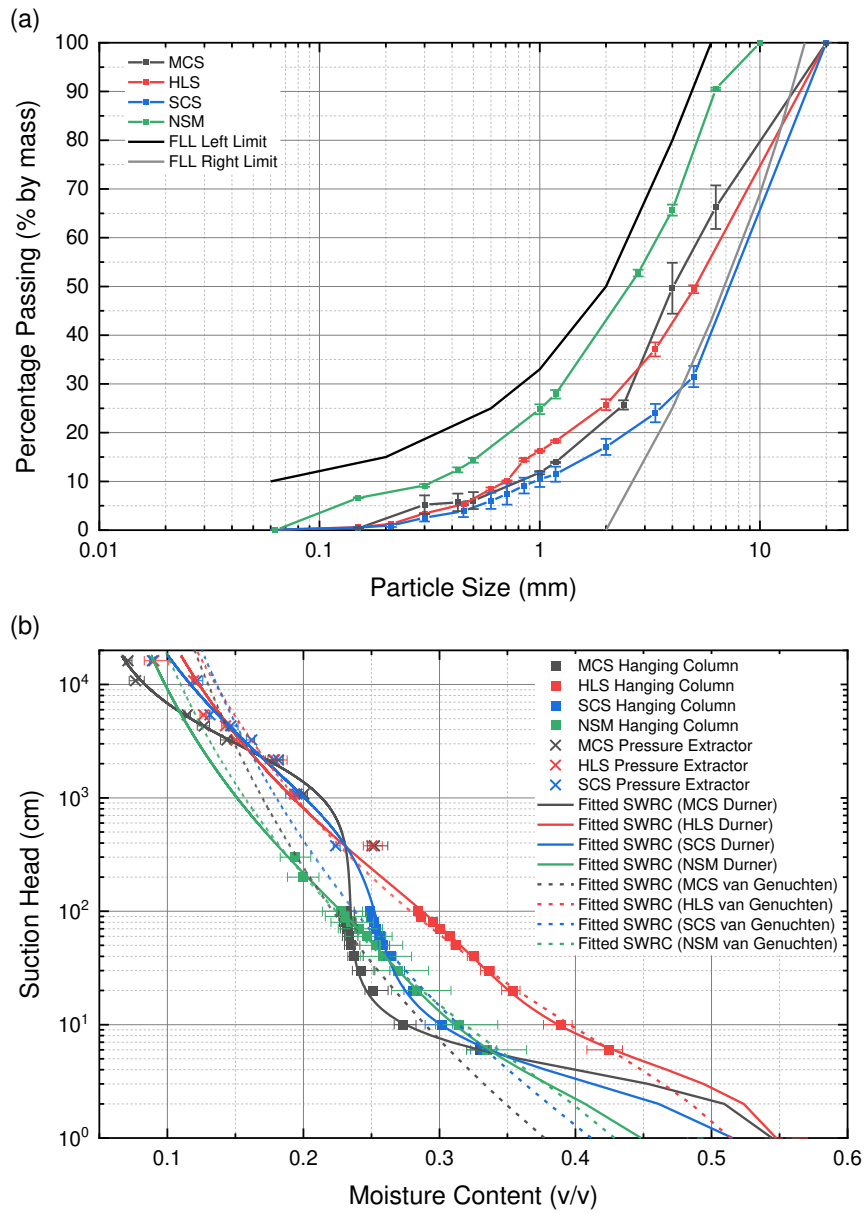


Fig. 3. Physical properties of the green roof substrates; (a) Particle Size Distribution (PSD); (b) Soil Water Release Curve (SWRC) (all graphs are plotted with the errors to the average values of the three tests to show the variation between test samples).

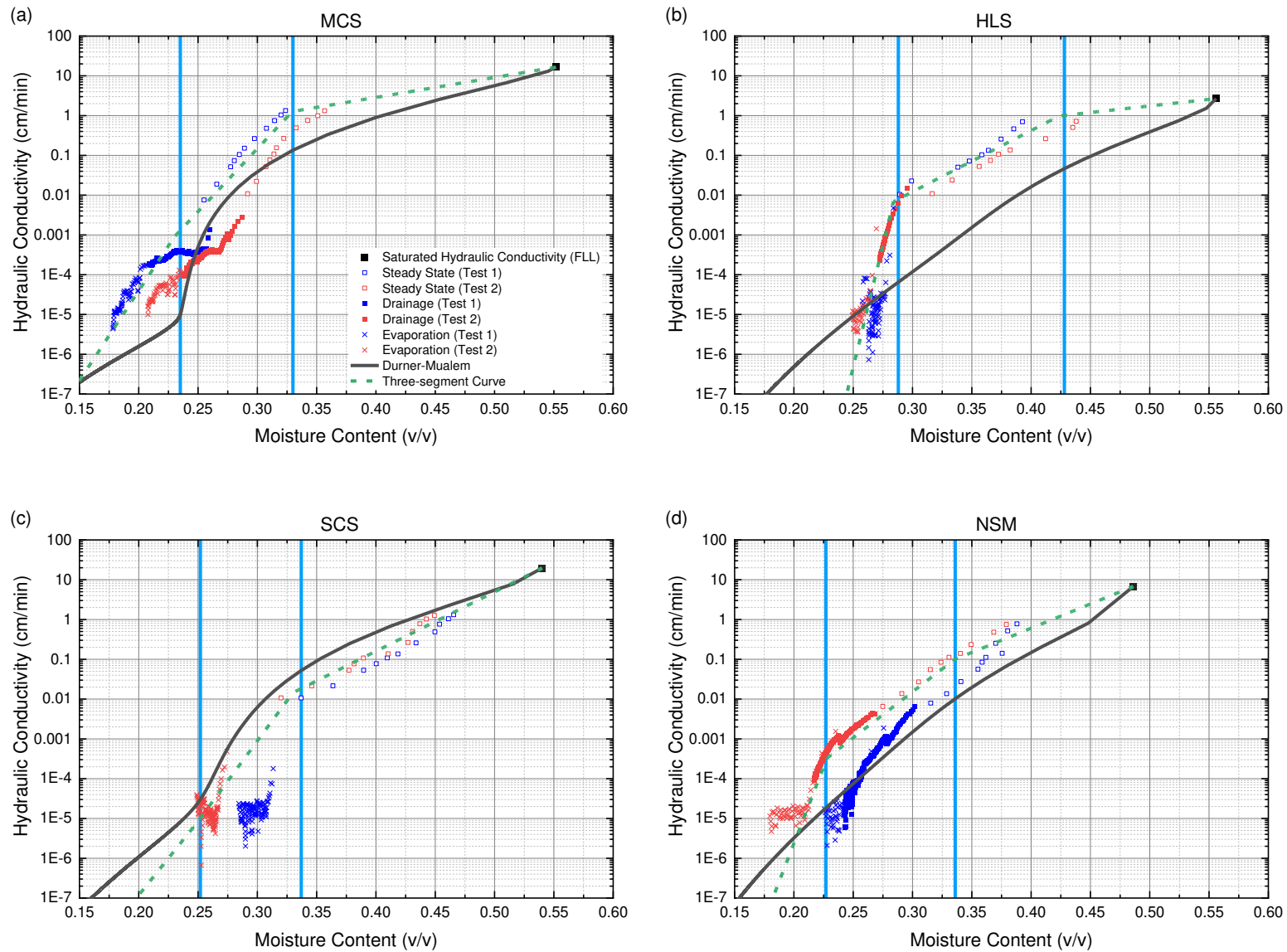


Fig. 4. Measured unsaturated hydraulic conductivity, estimated (Durner-Mualem model) and fitted (three-segment curve) hydraulic conductivity functions (HCFs) for the four substrates (the two vertical lines indicate the intercepts: the volumetric water content corresponding to 6 cm (right line) and 100 cm (left line) suction head).

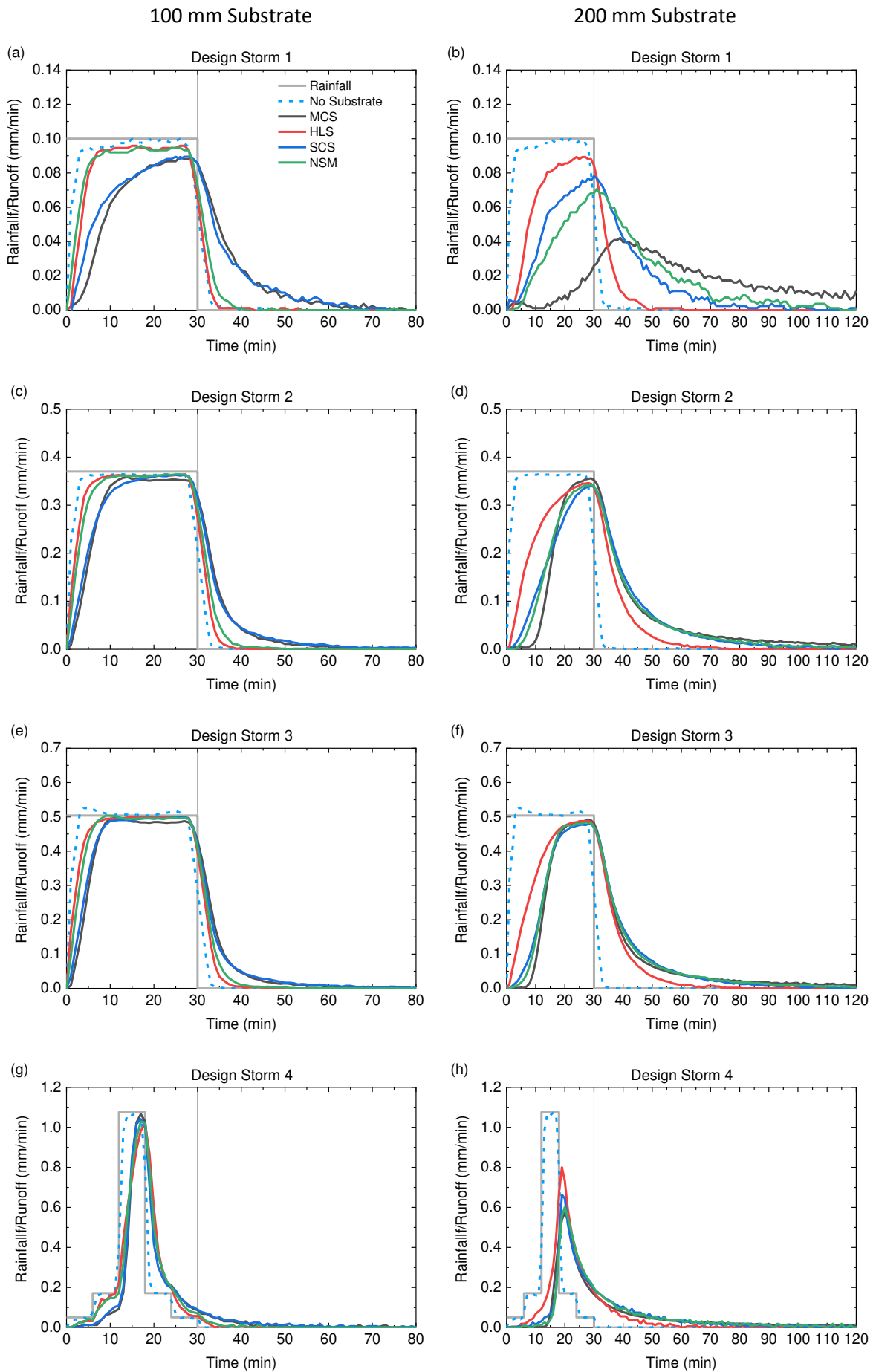


Fig. 5. Runoff profiles for the four trial substrates in response to four design storms (the vertical line indicates the end of the rainfall event).

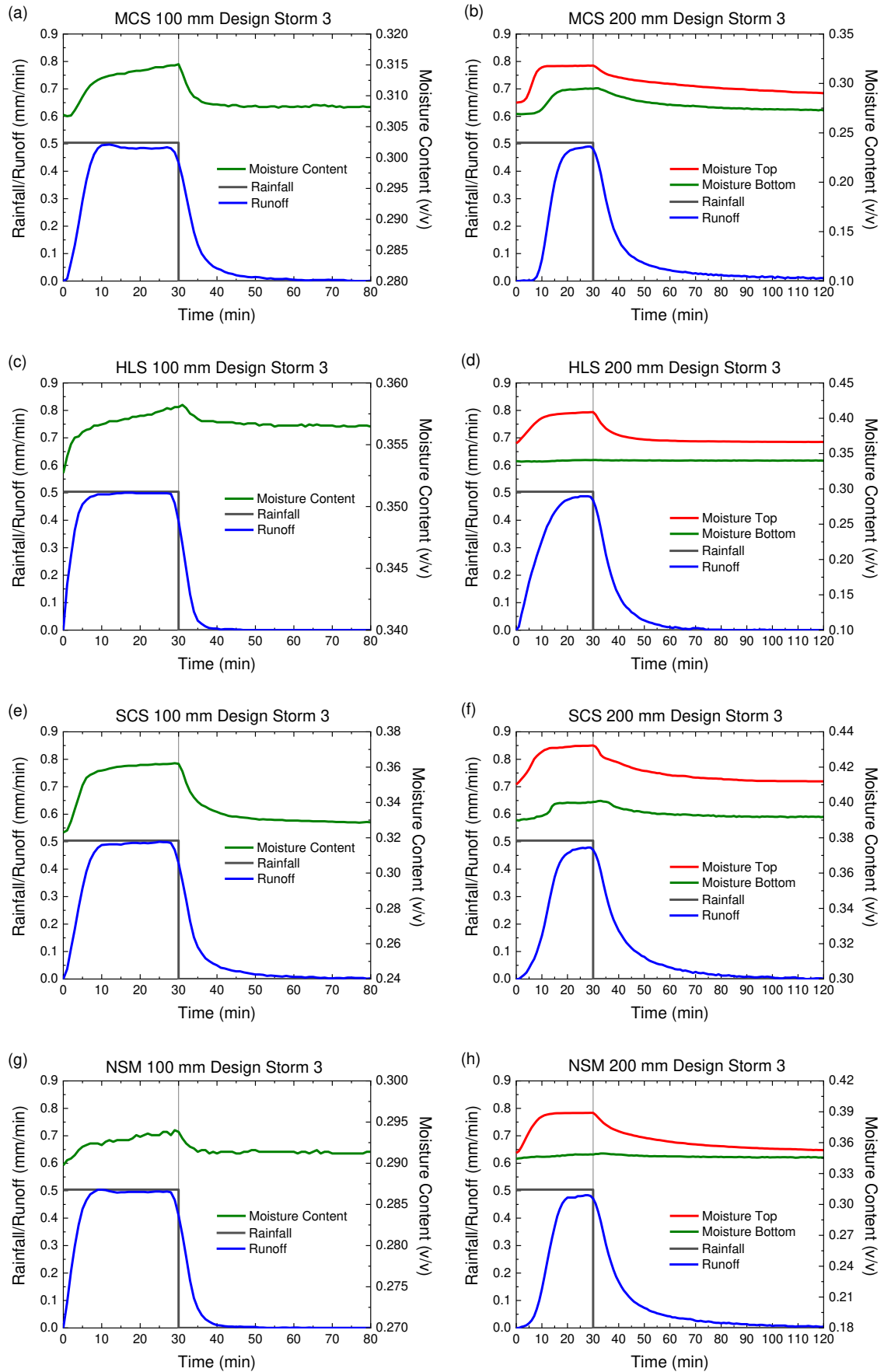


Fig. 6. Substrate moisture content profiles during Design Storm 3 (moisture content/ moisture bottom in the legend refers to the moisture content measured by P1 (Fig. 1) and moisture top refers to the data measured by P2 (Fig. 1); the vertical line indicates the end of the rainfall event and, to better present the dynamics within the substrate, the secondary Y axis range is not consistent).

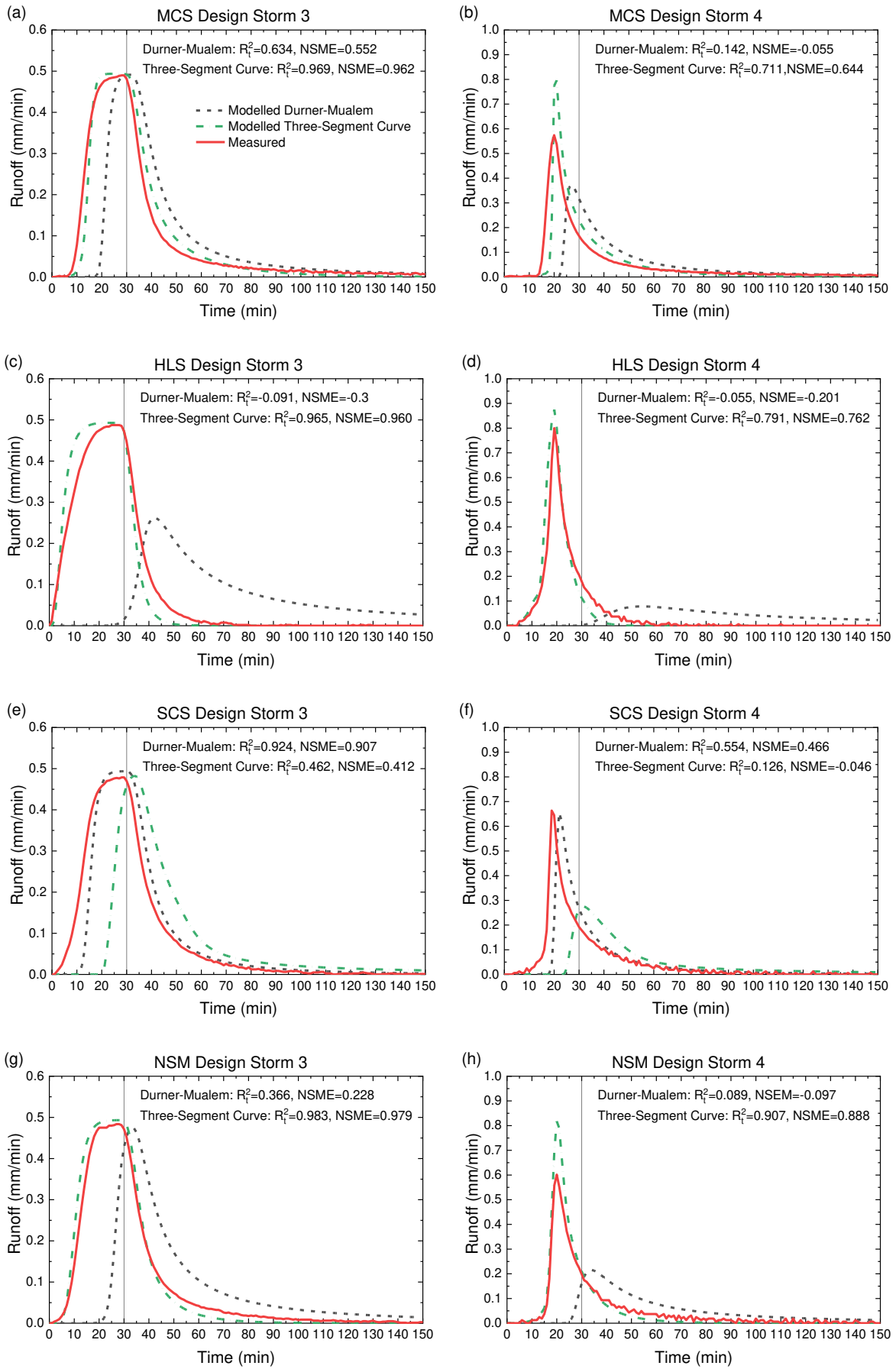


Fig. 7. Measured and modelled runoff profiles for the 200 mm substrates (the vertical line indicates the end of the rainfall event).

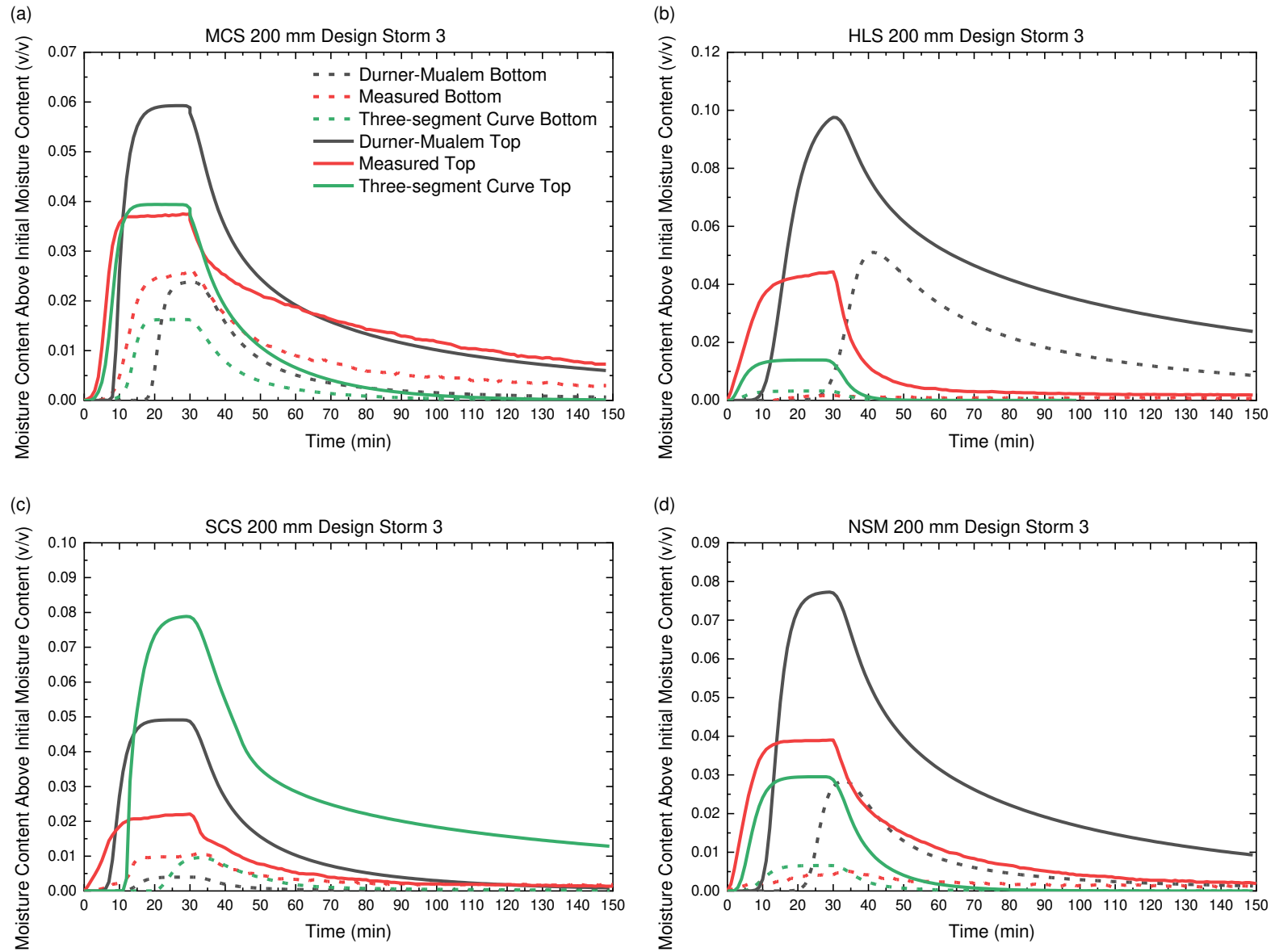


Fig. 8. Measured and modelled vertical moisture content profiles for the 200 mm substrates (bottom refers to the location of moisture probe P1 (Fig. 1) is and top refers to the location of P2 (Fig. 1)).

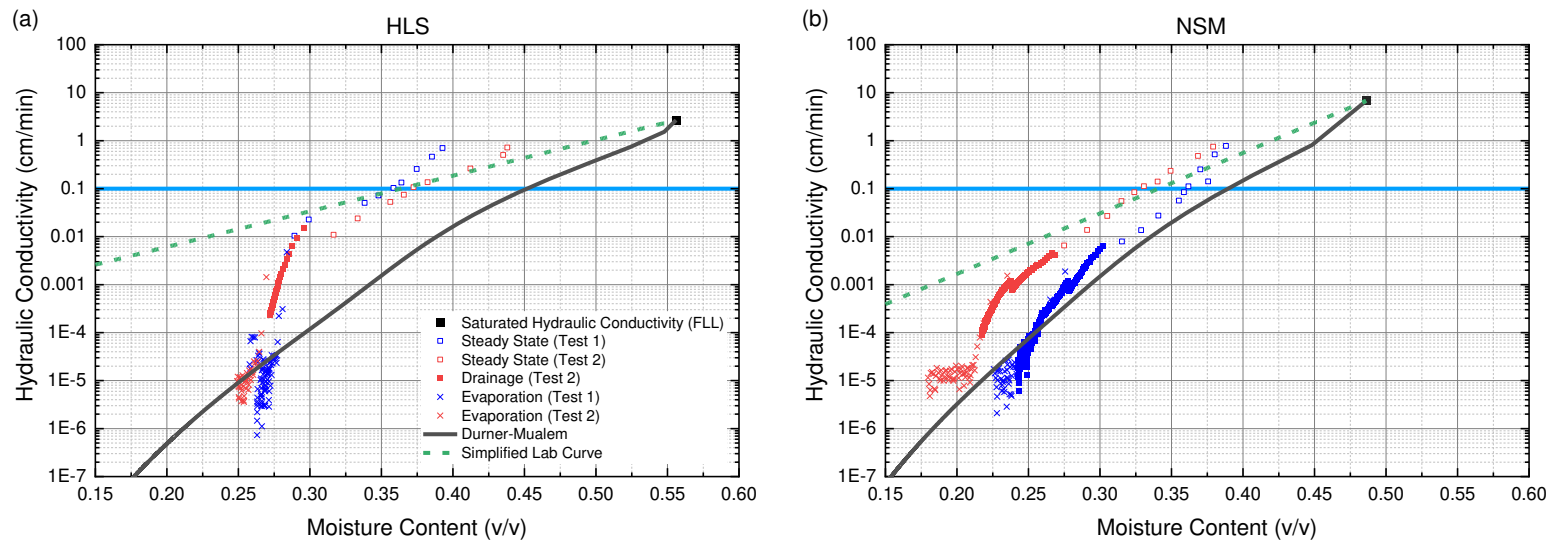


Fig. 9. Measured unsaturated hydraulic conductivity, estimated (Durner-Mualem model) and fitted (simplified lab curve) hydraulic conductivity functions for the two substrates (the horizontal line indicates the hydraulic conductivity of 0.1 cm/min).

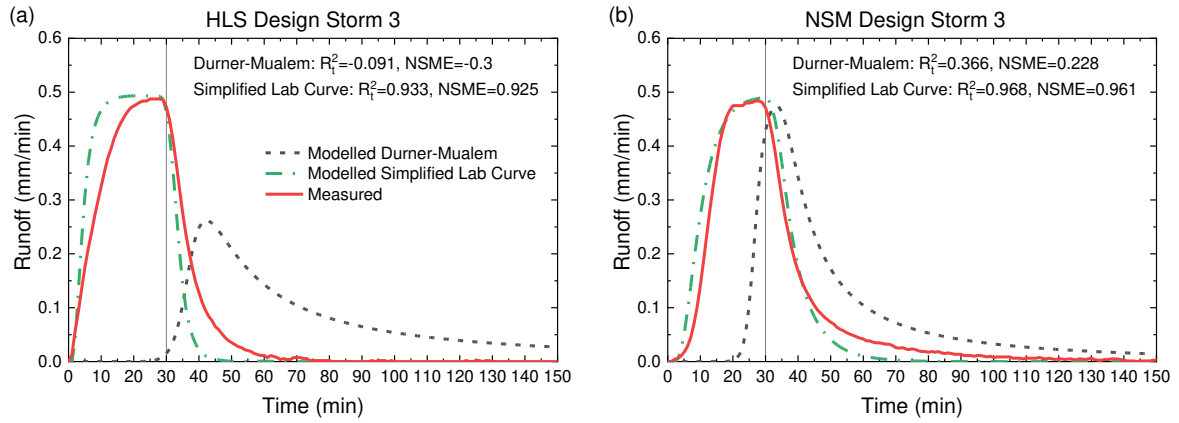


Fig. 10. Measured and modelled runoff profiles for the 200 mm substrates using the simplified lab curves (the vertical line indicates the end of the rainfall event).